J. Fluid Mech. (2002), *vol.* 468, *pp.* 239–270.
DOI: 10.1017/S0022112002001611 Printed in the United Kingdom

Baroclinic modon equilibria on the beta-plane: stability and transitions

By Z. KIZNER[1,2], D. BERSON[1] AND R. KHVOLES[2]

[1]Department of Physics, Bar-Ilan University, Ramat-Gam 52900, Israel

[2]Department of Mathematics Bar-Ilan University, Ramat-Gan 52900, Israel

(Received 24 September 2001 and in revised form 14 May 2002)

The objective of this work is a numerical study of the stability properties and the evolution of the eastward-travelling baroclinic modons – coherent vortex structures specific to stratified geophysical fluids where differential rotation (the β-effect) is of the essence. In the vortices under study, the initial dependence of the potential vorticity (PV) upon the streamfunction is piecewise-linear, the barotropic component is dipolar, the baroclinic component is circularly symmetric about the vertical axis, and the boundary of the trapped-fluid region (in which the vorticity contours are closed) is a circular cylinder. These modons are shown to be stable for a wide range of parameters. In two- and three-layer fluids, modons of this type are shown to be able to transit to even more durable states, in which the trapped-fluid area is oval in shape and the PV versus streamfunction dependence in this domain is nonlinear. Possible transition mechanisms and linkage between the circular and oval modons are discussed.

1. Introduction

Today, the crucial role of mesoscale vortices in the dynamics of oceans and atmosphere is widely recognized. Mesoscale vortices are present everywhere in the World Ocean (e.g. Wirtki, Magaard & Hager 1976; Richardson 1983*a*; Ikeda, Mysak & Emery 1984; Ikeda & Emery 1984; Kamenkovich, Koshlyakov & Monin 1986, chap. 1; Hecht, Pinardi & Robinson 1988; Hooker *et al.* 1995). Observations show that oceanic mesoscale eddies can survive for a long time with small dispersion and slow decay. This has been shown, for instance, for eddies in the Gulf Stream (Richardson 1983*b*) and the Mediterranean (Feliks & Itzikowitch 1987; Hecht *et al.* 1988). The long lifespan of these eddies motivated researchers to look for the stationary solutions that are considered below.

Exact and asymptotic solutions representing steadily travelling shape-preserving localized vortices on the β-plane were derived for both barotropic and stratified fluids (e.g. Stern 1975; Larichev & Reznik 1976*a*, *b*; Berestov 1979; Flierl *et al.* 1980; Mied & Lindemann 1982; Tribbia 1984; Verkley 1984; Reznik 1985; Kizner 1984*a*, *b*, 1986*a*, *b*, 1988, 1997; Pakyari & Nycander 1996). These solutions are referred to as modons. A modon carries the fluid trapped in its core and travels along a parallel. Conventional modons are strongly localized; their characteristics decay exponentially in space, the exponent being dependent on the translation speed. The simplest modon is a barotropic dipole current system, while some dipole (or, more generally, antisymmetric) component is always present in any modon, forcing it to propagate.

In a truly stationary localized vortex, outside its core, the dependence between the potential vorticity (PV) and the streamfunction (considered in the frame travelling along with the vortex) is a simple proportionality (Larichev & Reznik 1976*a*; see also Flierl *et al.* 1980), while inside the region of trapped fluid it can be, generally speaking, nonlinear. However, for the exact modon solutions on the β-plane known to date, this interior dependence is linear, the trapped-fluid region being circular. Boyd & Ma (1990) considered free elliptical dipoles on the f-plane, where the β-effect is absent (see also Hesthaven *et al.* 1995). They showed numerically that although in order to provide elliptical modons the interior PV vs. streamfunction relationship must be nonlinear, it is linear for circular modons. This appears to be true for the β-plane as well, but to date there has been only partial evidence in favour of this analogy. Haupt, McWilliams & Tribbia (1993) considered approximately circular barotropic numerical modon solutions in weak symmetric shear flow on the β-plane and found the interior PV *vs.* streamfunction relationship to be linear. This was also a characteristic property of the barotropic diploes that emerged from collapsing vortical structures in the numerical experiments of Kizner & Berson (2000). In numerical experiments of McWilliams & Zabusky (1982), two merging Larichev–Reznik dipoles created a quasi-stationary vortex with a nonlinear interior relationship, but the form of the trapped-fluid area was not determined. The issue of the existence of baroclinic non-circular modons and modons with nonlinear interior PV vs. streamfunction relationships has not been considered until now.

Observations of dipole vortices are available in both the ocean and atmosphere (e.g. Ikeda *et al.* 1984; Ikeda & Emery 1984; Hooker *et al.* 1995; McWilliams 1980; Butchart, Haines & Marshall, 1989). Nevertheless, the major part of the observed mesoscale vortices can be characterized as nearly axisymmetric monopoles rather than dipoles (Kamenkovich *et al.* 1986, chaps. 4, 5; Olson 1980, 1991). This was the motivating factor in seeking the so-called 'dipole-plus-rider' modon solutions, in which the circularly symmetric 'rider' component can mask the dipole pattern.

The rider PV in barotropic dipole-plus-rider solutions (Flierl *et al.* 1980; Berestov 1981) is discontinuous. Swenson (1987) showed the instability of such solutions. In two-layer numerical experiments, McWilliams & Flierl (1979) and Mied & Lindemann (1982) showed that baroclinic dipole-plus-rider modon-like structures (with a continuous PV field) could result from evolving baroclinic monopoles and hetons (this term was first used by Hogg & Stommel (1985) to designate a baroclinic vortex pair formed by vortices located in different layers of a two-layer fluid and separated by a certain distance). Similar results were obtained by Feliks (1990) in two- and four-mode quasi-geostrophic numerical experiments on the evolution of an initially Gaussian baroclinic monopole. The simulations in these works were carried out for relatively short times (a few tens of synoptic periods). Feliks & Ghil (1993, 1996), using a quasi-geostrophic model, showed that eddies detached from boundary currents do exhibit the structure of a barotropic dipole with a baroclinic rider. Pakyari & Nycander (1996) suggested a two-layer asymptotic dipole-plus-rider solution and provided some qualitative argumentation in favour of the stability of the eastward-travelling baroclinic dipole-plus-rider modons.

For continuously stratified fluid, Kizner suggested different types of exact (1984*a*, 1988, 1997) and asymptotic (1986*a*, *b*) solutions of the dipole-plus-rider type with a piecewise PV *vs.* streamfunction relationship and a continuous PV field (below identified as smooth modons); some of them (1984*a*, 1986*a*, 1997) can be fitted to any stratification and are therefore of special interest. The barotropic mode, in these solutions, coincides with the barotropic modon of Larichev & Reznik (1976*a*) and

the amplitude of the axisymmetric baroclinic rider is arbitrary, the trapped-fluid area being a circular cylinder.

Long lifespans of the dipole barotropic modons (especially those travelling east) have been demonstrated numerically (McWilliams *et al.* 1981; Makino, Kamimura & Taniuti 1981; Larichev & Reznik 1982, 1983; McWilliams & Zabusky 1982; Hesthaven, Lynov & Nycander 1993) and in laboratory experiments (Flierl, Stern & Whitehead 1983; Velasco Fuentes & van Heijst 1994, 1995). In the present work, the stability properties and long-term evolution of smooth circular baroclinic modons are studied numerically, the specific questions addressed being the following: Can modons of this type be stable? What are the ranges of the parameters that admit durable modons? What are the mechanisms of the modon unstable evolution? Are there some stationary coherent regimes that differ from circular modons? If so, what are they? Are they somehow linked to the circular modons? A multi-layer quasi-geostrophic model is initialized using the above-described exact baroclinic circular modon solutions at different translation speeds and rider amplitudes, and forward integration is conducted for super long times (up to 2000 synoptic periods). We consider in detail the case where the unperturbed layer depths are the same, and the density jumps between the layers are equal ('linear' stratification).

In the next section, the main concepts are introduced. In § 3, we describe the numerical approach applied. The experiments on the evolution of baroclinic modons conducted with the use of the two- and three-layer versions of the numerical model are presented and discussed in § 4.

2. Background

We base our considerations on the principle of conservation of PV in the quasi-geostrophic approximation.

In a Cartesian coordinate system attached to a point at some reference latitude so that the x-axis is directed eastward, y – northward, z – upward ($z = 0$ at the non-perturbed free surface), the conservation of the quasi-geostrophic PV is given by the equations:

$$\frac{\partial q}{\partial t} + J(\psi, q) = 0, \tag{1}$$

$$q = \Delta\psi + \frac{\partial}{\partial z}\left[\frac{f_0^2}{N^2}\frac{\partial \psi}{\partial z}\right] + \beta y. \tag{2}$$

Here, J is the Jacobian; Δ is the Laplacian in x and y; ψ is the streamfunction for the horizontal velocity components ($u = -\partial\psi/\partial y$, $v = \partial\psi/\partial x$); q is the PV; $f = f_0 + \beta y$ is the Coriolis parameter, where f_0 is the reference-latitude inertial frequency, β is the meridional gradient of f; $N = \sqrt{(g/\rho_s)(\mathrm{d}\rho_s/\mathrm{d}z)}$ is the Brunt–Väisälä frequency characterizing the non-perturbed stratification, $\rho_s = \rho_s(z)$ is the ambient density profile, and g is the acceleration due to gravity.

The typical horizontal scale of oceanic synoptic eddies, which are the main subject of our study, is equal to the internal Rossby radius, $L_{Ro} = (\overline{N}/f_0)H \sim 50\,\mathrm{km}$ (where $\overline{N}$ is the average Brunt–Väisälä frequency). For the currents of such a scale the 'rigid-lid' condition at the free surface, i.e. the equality to zero of the vertical velocity component at $z = 0$, is valid to a high level of approximation (Kamenkovich *et al.* 1986, chap. 2). We will accept the same condition at $z = H = const$ regarding the

bottom as flat (and non-sloping). These conditions are obeyed if we assume that

$$\frac{\partial \psi}{\partial z} = 0 \quad \text{at} \quad z = 0, -H. \tag{3}$$

The so-called vertical normal modes, $F^{(j)}(z)$, are further introduced as the eigenfunctions of the 'vertical operator' appearing in equation (2) that obey the conditions (3). These are the solutions of the Sturm–Liouville problem

$$\frac{\mathrm{d}}{\mathrm{d}z}\left(\frac{f_0^2}{N^2}\frac{\mathrm{d}}{\mathrm{d}z}F\right) + m^2 F = 0, \quad F'(0) = F'(-H) = 0. \tag{4}$$

If the stratification is stable ($N^2 > 0$) and N^2 is a differentiable function, then (4) has an infinite set of eigenvalues, $0 = m_0^2 < m_1^2 < m_2^2 < \ldots$, the eigenfunctions being mutually orthogonal (e.g. Kamke 1959). In the n-layer model, i.e. when $\rho(z)$ is a piecewise-constant function, there are only n vertical modes, which are piecewise-constant functions of z (Kamenkovich *et al.* 1986, chap. 2). In this case, it is appropriate to replace the notations $\psi = \psi(x, y, z, t), q = q(x, y, z, t)$, and $F^{(j)}(z)$ by $\psi_i = \psi_i(x, y, t)$, $q_i = q_i(x, y, t)$, and $F_i^{(j)}$, respectively, where i is the layer index. The vertical normal modes for the n-layer model can be obtained in the framework of the general approach (equations (2)–(4)) if the Brunt–Väisälä frequency is understood as a superposition of $n - 1$ Dirac functions. This fact allows us to refer to equation (2) regardless of whether a continuous or multi-layer stratification is considered. Note that $F^{(0)} = const$, whereas each function $F^{(j)}$ at $j > 0$ changes its sign j times and its integral over the depth is zero. The zero mode is conventionally called barotropic, whereas the remaining modes are called baroclinic.

Clearly, any solution to (1)–(3) can be represented in the form

$$\psi = \sum_{j=0}^{n-1} \psi^{(j)}(x, y, t) F^{(j)}, \quad q = \sum_{j=0}^{n-1} q^{(j)}(x, y, t) F^{(j)}, \tag{5}$$

where n is either finite (n-layer model) or infinite (continuous stratification). Substitution of (5) into (2) implies the following equations:

$$q^{(0)} = \Delta \psi^{(0)} + \beta y, \quad q^{(j)} = \Delta \psi^{(j)} - m_j^2 \psi^{(j)} \quad (j = 1, 2, \ldots, n-1). \tag{6}$$

Here, we are interested in vortices that, in addition to the barotropic mode, contain only one, say j_0th, baroclinic mode. In this case, (5) and (6) are reduced to

$$\psi = \psi_{BT}(x, y, t) + \psi_{BC}(x, y, t) F_{BC}, \quad q = q_{BT}(x, y, t) + q_{BC}(x, y, t) F_{BC}, \tag{7}$$

$$q_{BT} = \Delta \psi_{BT} + \beta y, \quad q_{BC} = \Delta \psi_{BC} - m_{j_0}^2 \psi_{BC}, \tag{8}$$

where the following notations are used: $\psi^{(0)} = \psi_{BT}$, $\psi^{(j_0)} = \psi_{BC}$, $F^{(j_0)} = F_{BC}$.

If the vortex propagates steadily in the x-direction at a translation speed U then, in the travelling coordinate frame ($x \to \tilde{x} = x - Ut$), equation (1) will be reduced to

$$J(\Psi, q) = 0, \quad \Psi = \psi + Uy. \tag{9}$$

In these coordinates, streamlines – isolines of Ψ – are the pathways of the fluid particles, i.e. lines of constant PV. Accordingly, equations (9) mean that, in such a vortex, PV is a certain (as yet arbitrary) function of Ψ and z. (In the case of a multi-layer fluid, q_i is a function of Ψ_i, and this function can vary for different i.) Note that, in general, equations (9) do not automatically secure a relationship between q_{BT} and $\Psi_{BT} = \psi_{BT} + Uy$ or between q_{BC} and $\Psi_{BC} = \psi_{BC}$.

Localization means that the function ψ abates quite rapidly at the periphery and thus $\Psi \to Uy$ and $q \to \beta y$ at $\tilde{x} \to \infty$. This immediately implies that far enough from the vortical core, at sufficiently large values of $r = \sqrt{\tilde{x}^2 + y^2}$, the isolines of the functions Ψ and q are open and, in the region of open isolines, PV is simply proportional to Ψ. First, following Flierl *et al.* (1980), we will consider a solution in which, at any z, the contour demarcating the regions of closed and open isolines is a circle of the same radius a, so that

$$q = l^2\Psi, \quad r > a, \tag{10}$$

where

$$l^2 = \beta/U. \tag{11}$$

In the exterior region, the proportion holds separately for q_{BT} and Ψ_{BT}, on the one hand, and q_{BC} and Ψ_{BC}, on the other. Analysis shows that localized solutions to (2), (10) and (11) that contain the barotropic mode exist only if $l^2 > 0$. This means that, under the rigid-lid conditions (equation (3)), such localized vortices propagate only eastwards (e.g. Larichev & Reznik 1976*a*, *b*; Flierl *et al.* 1980; Kizner 1997). Regarding the interior, trapped-fluid region $r < a$, we will assume that the dependence of q upon Ψ is linear:

$$q = -k^2\Psi + DF_{BC}, \tag{12}$$

where k^2 and D are constants (non-circular vortices with nonlinear relationships between q and Ψ will be discussed in § 4).

The conditions for matching the exterior and the interior solutions are those of continuity of the pressure (ψ), velocity and PV fields at the contour $r = a$. Using (7), an exact circular modon solution that satisfies equations (5), (10) and (12) and fits any stratification can be represented in the polar coordinates r, θ in the form (Kizner 1997):

$$\psi_{BT} = \Phi_{BT}(r)\sin\theta, \quad \psi_{BC} = \Phi_{BC}(r), \tag{13}$$

$$\Phi_{BT} = \begin{cases} U\left[a\dfrac{l^2}{k^2}\dfrac{J_1(kr)}{J_1(ka)} - \left(\dfrac{l^2+k^2}{k^2}\right)r\right] & (r < a) \\ -aU\dfrac{K_1(lr)}{K_1(la)} & (r > a), \end{cases} \tag{14}$$

$$\Phi_{BC} = \begin{cases} A\left[J_0(k_{j_0}r) - \dfrac{l^2+k^2}{l_{j_0}^2}J_0(k_{j_0}a)\right] & r < a) \\ -A\dfrac{k_{j_0}^2}{l_{j_0}^2}\dfrac{J_0(k_{j_0}a)}{K_0(l_{j_0}a)}K_0(l_{j_0}r), & (r > a). \end{cases} \tag{15}$$

Here, J_v and K_v are v-order Bessel and Macdonald functions, A is a free coefficient,

$$l_{j_0} = \sqrt{l^2 + m_{j_0}^2}, \quad k_{j_0} = \sqrt{k^2 - m_{j_0}^2}, \tag{16}$$

and parameters a, k, l, k_{j_0} and l_{j_0} are related by the equations

$$-k\frac{J_1(ka)}{J_2(ka)} = l\frac{K_1(la)}{K_2(la)}, \quad -k_{j_0}\frac{J_0(k_{j_0}a)}{J_1(k_{j_0}a)} = l_i\frac{K_0(l_{j_0}a)}{K_1(l_{j_0}a)}. \tag{17}$$

In this solution, the barotropic mode is antisymmetric about the x-axis and the baroclinic mode is circularly symmetric about the vertical axis. In view of (11),

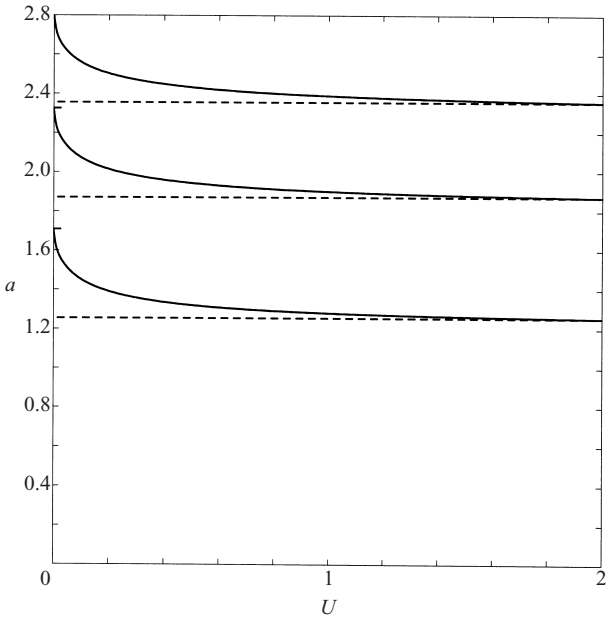

FIGURE 1. Dispersion relationship (radius vs. translation speed) for the smooth solution given by equations (7) and (13)–(17). The lower branch corresponds to the modons composed of a barotropic dipole and a baroclinic monopole.

equations (16) and (17) determine the dispersion relationship for the smooth solution given by equations (7) and (13)–(17) – the dependence of the vortex radius a upon its translation speed U. Since functions J_1 and J_2 alternate, whereas K_1 and K_2 do not, this relationship is many-valued (figure 1).

Here, we will consider only the modon solutions based on the lower branch of the dispersion relationship; this is exactly the case when the barotropic mode is a dipolar modon of Larichev & Reznik (1976*a*) and the baroclinic mode, at each z, is a smooth monopolar rider. (Higher branches correspond to the so-called shielded modons. In this case the barotropic mode is multipolar, which yields instability of the modon, Kizner & Berson 2000.) Most of the following considerations will be limited to the modons that carry riders in the first baroclinic mode ($j_0 = 1$). As the first mode, $F^{(1)}$, changes sign once over the interval $0 < z < -H$, such a solution, in fact, is heton-like: the PV peak values are assumed at $z = 0, -H$ and are moved apart in the y-directions. The nonlinear interaction between the upper and bottom vortices causes the propagation of the entire vortex system eastwards and its possible coherence. However, the fact that the solution (7) and (13)–(17) allows arbitrary (even zero) amplitude A of the baroclinic mode, means that the overall transport of the vortex structure is conditioned by the barotropic dipole – by its size and intensity. At the same time, the presence of a smooth rider imposes an additional constraint on the parameters of the barotropic dipole – the dependence between its size and translation speed (and thus, the dependence between size and intensity).

The general objective of our investigation is to examine the stability properties of the modons given by equations (7) and (13)–(17), the specific questions addressed in the present paper being formulated in § 1. The task being faced can hardly be managed using analytical methods only. On the other hand, a numerical study is

facilitated by the fact that the solution (7) and (13)–(17) is valid for a multi-layer fluid.

3. Numerical multi-layer model

Our computer model is based on the non-dimensional versions of equations (1) and (2) for the n-layer fluid. The scales used are: $L_{Ro} \approx 50\,\mathrm{km}$ and $T = 1/\beta L_{Ro} \approx 10$ days, for the space and time variables x, y, t (synoptic scales); βL_{Ro}^3 and βL_{Ro}, for the streamfunction and potential vorticity, respectively. Equations (1) and (2) are integrated in a rectangular domain $[-X < x < X; -Y < y < Y]$. Periodicity conditions are applied at $x = \pm X$, while the boundary conditions at $y = \pm Y$ are $\partial\psi^{(j)}/\partial x = 0$ and $\int_{-X}^{X}(\partial^2\psi^{(j)}/\partial t\partial y)\,\mathrm{d}x = 0$ (Buchwald 1973; Larichev 1974; see also Kamenkovich *et al.* 1986, chap. 2). In the experiments presented below, $X = Y = 15L_{Ro}$ and the mesh size is $\delta = 0.1L_{Ro}$; the time step τ is controlled by the gradients of ψ and q and does not exceed $2.5 \times 10^{-3}T$. Most of the experiments are run with the solution (7) and (13)–(17) specified as an initial condition (at different translation speeds and amplitudes of the baroclinic mode).

Briefly, the computational algorithm is as follows. At any moment $t > 0$, in each layer, PV is computed from a finite-difference analogue of equation (1) with the use of a combination of the direct and Matsuno schemes and Arakawa approximation for the Jacobian operator (Mezinger & Arakawa 1976), the streamfunction being taken from the previous moment, $t-\tau$. Subsequently, the layer streamfunctions ψ_i are determined ($i = 1, \ldots, n$). At this stage, PV is expanded into a linear combination of vertical normal modes according to (5), and n finite-difference analogues of independent equations (6) in $\psi^{(j)}$ are solved ($j = 0, \ldots, n-1$) using decomposition into eigenfunctions in the x-direction and marching in the y-direction (Samarsky 1989). Such a scheme affords conservation of the integral vorticity while, according to our tests, the conservation of the total energy and enstrophy is held within 0.5% each until $2000T$.

While travelling eastwards, the vortex can encounter its own vortical filaments and Rossby waves radiated by itself that enter the basin through the eastern boundary owing to the periodicity in the x-direction. To avoid such head-on interactions, we adopt the so-called cutting procedure (Hesthaven *et al.* 1993), according to which, periodically in time, a mask is put on the computed streamfunction field, the period being equal to T. This procedure does not change the ψ field within the area $r < 5L_{Ro}$, but reduces it smoothly to zero in the periphery. Clearly, when this procedure is applied, the integral vorticity, enstrophy and energy can be conserved only within the period T, between the subsequent cuttings. Our experiments showed that the computational algorithm described above allows the study of super long-term evolution of vortical structures.

Barotropic Larichev–Reznik modons travelling east at the translation speeds 0.3 to $1.2L_{Ro}/T$ were used to test the numerical model. The changes in their parameters and structure were insignificant until $\sim 500T$. In dipoles whose initial translation speeds were small, weak slowing down of the eastward drift caused by the numerical effects (for discussion see §4.1.1) led to the loss of coherence at long times ($t > 1500T$).

For the purposes of our investigation, plural high-resolution long-term computations are required. Note also that in a multi-layer model, the volume of the calculations required exceeds greatly that needed in a barotropic model. Therefore, at the present stage, we confine ourselves to two- and three-layer dipole-plus-rider modons (two-layer structures of this type were first considered by Mied & Lindemann, 1982),

the space resolution being $\delta = 0.1L_{Ro}$. Two re-run experiments that lasted for $400T$ were conducted with a tilted circular modon at $\delta = 0.1L_{Ro}$ and $\delta = 0.075L_{Ro}$ (and appropriately reduced time step), but no significant difference in results was observed (the experiment at $\delta = 0.1L_{Ro}$ is presented in § 4.1.2).

4. Results and discussion

4.1. *Two-layer modons*

4.1.1. *Overview*

In a two-layer fluid, which will be considered first, $F_{BC} = F^{(1)}$. For definiteness we will regard the vertical modes normalized in such a way that $F^{(0)} = 1$ and $F_1^{(1)} = 1$; this implies that $F_2^{(1)} = -\varepsilon$, where $\varepsilon = h_1/h_2$ is the ratio between the depths of the layers. Without loss of generality, we may assume that $\varepsilon \leqslant 1$ (if otherwise, the layer indices can be interchanged). Using (1) and (7), we arrive at the following equations describing the evolution of the barotropic and baroclinic components of PV:

$$\frac{\partial}{\partial t} q_{BT} + J(\psi_{BT}, q_{BT}) + \varepsilon J(\psi_{BC}, q_{BC}) = 0, \tag{18}$$

$$\frac{\partial}{\partial t} q_{BC} + J(\psi_{BT}, q_{BC}) + J(\psi_{BC}, q_{BT}) + (1-\varepsilon) J(\psi_{BC}, q_{BC}) = 0. \tag{19}$$

The case $\varepsilon = 1$, when the layers are of the same thickness, is of particular interest. As seen from equations (8), (18) and (19), in this case, the antisymmetry of the barotropic mode and the symmetry of the baroclinic mode, which are inherent characteristics of the solution (7) and (13)–(17), are retained during the evolution of the vortex. A consequence of this symmetry/antisymmetry is that if, in a steady state reached in the course of the vortex evolution, the trapped-fluid regions in the upper and the lower layer are the same, their common boundary coincides with the zero contour of q_{BT} (and, therefore, with the contour $\Psi_{BT} = 0$), thus being symmetric about the x-axis. These facts make the vortex evolution especially accessible for analysis, and we will focus our consideration primarily on this case. Such a two-layer stratification represents an analogy to a linear stratification in a continuously stratified fluid, and will be referred to below as 'linear' stratification. Note that, in a continuously stratified fluid, equations (18)–(19) at $\varepsilon = 1$ describe the evolution of the barotropic and first baroclinic modes in the two-mode approximation if the stratification is linear and the modes are normalized so that $F^{(0)} = 1$ and $F^{(1)}(0) = \sqrt{2}$. Thus, the results presented in §§ 4.1.1–4.1.3 remain valid in this approximation.

Some results of a simulation, in which the initial state is characterized by a unit translation speed and the baroclinic mode is 3 times stronger than the barotropic mode ($A_{BC}/A_{BT} = \max|\psi_{BC}|/\max|\psi_{BT}| = 3$), are shown in figures 2–8. The simulation lasted until $1800T$, and the total energy changed within a 3% interval during this period, the change being due mainly to the cutting procedure applied. Accordingly, no essential loss of total enstrophy E was observed (figure 2*a*), except for two short intervals of relatively small enstrophy lowering (2.7% and 2%, respectively). The latter indicate some significant restructuring of the vortex system attended by emission of vortical filaments and patches (which escape from the domain under consideration). It is seen that, almost immediately, the total potential energy P sinks noticeably, and then nearly stabilizes for more than $200T$ (which is more than 5 years for the chosen scales); thereafter, it again drops drastically, levels off and scarcely changes until the end of the experiment (figure 2*b*). As opposed to the small changes in the total

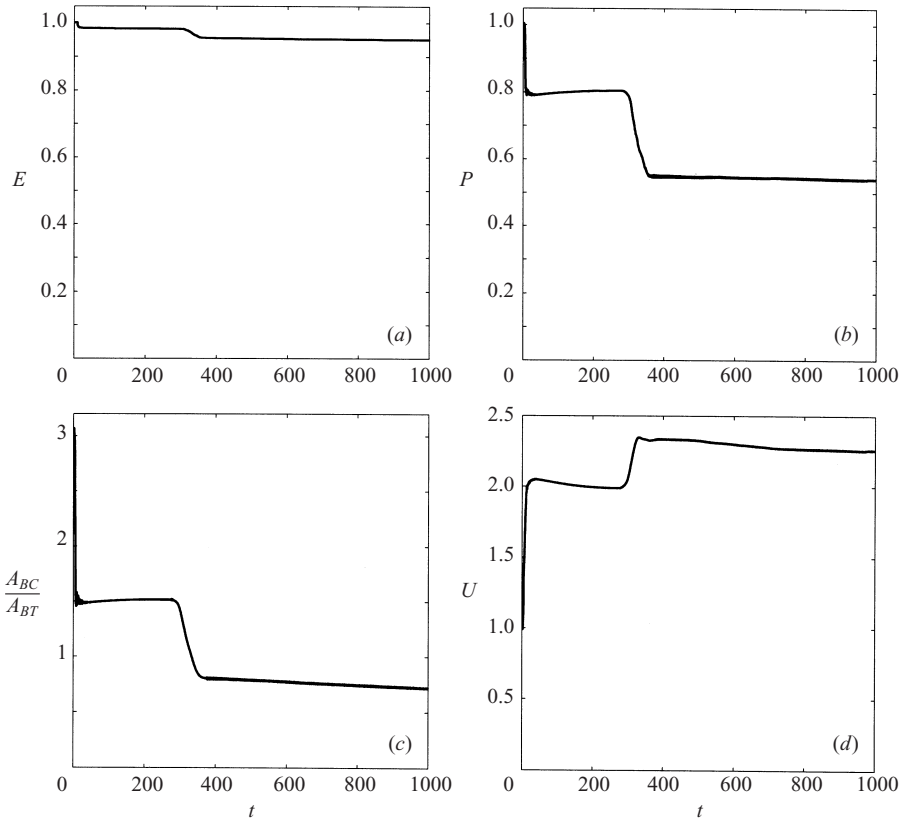

FIGURE 2. Evolution of a modon in the two-layer 'linearly' stratified fluid; the initial state is given by equations (7) and (13)–(17) at $U = 1$ and $A_{BC}/A_{BT} = 3$. (*a*) Total enstrophy normalized with the initial value. (*b*) Total potential energy normalized with the initial value. (*c*) Baroclinic-to-barotropic amplitude ratios. (*d*) Translation speed. Time t is given in synoptic periods T and speed in L_{Ro}/T.

energy, the steep descents in the potential energy are significant and are indicative of an energy transfer from the baroclinic mode to the barotropic mode. This conclusion gains substance from the analysis of the dynamics of the baroclinic-to-barotropic amplitude ratio, A_{BC}/A_{BT}, these being quite similar to those of the potential energy (figure 2*c*). At the same time, the translation speed U rises sharply, stabilizes, then again increases and stabilizes, although some slowing down can be observed in the stages of quasi-stationary eastward translation (figure 2*d*). This evidence allows us to speak of two transitions undergone by the vortex and two quasi-stable states attained. Although we cannot rule our some possible physical factors in the observed vortex hindering, our tests suggest that it is mainly due to the numerical effects.

The formation of a low-value 'extra' vorticity train behind a travelling vortex common to finite-difference numerical models (van Geffen & van Heijst 1998) is one of the hindering factors. Another contributor to this hindering is the periodically applied cutting (as noted by Hesthaven *et al.* 1993). It damps out to some extent the external streamfunction and PV fields. In terms of the stationary exterior fields (see the lower lines in equations (14) and (15)) this is equivalent to some increase in l and, owing to relationship (12), to a decrease in the translation speed. Thus, we might conclude that, while at the non-stationary stages of the modon evolution (such as the above transitions) the cutting minimizes the effects caused by the x-periodicity of the

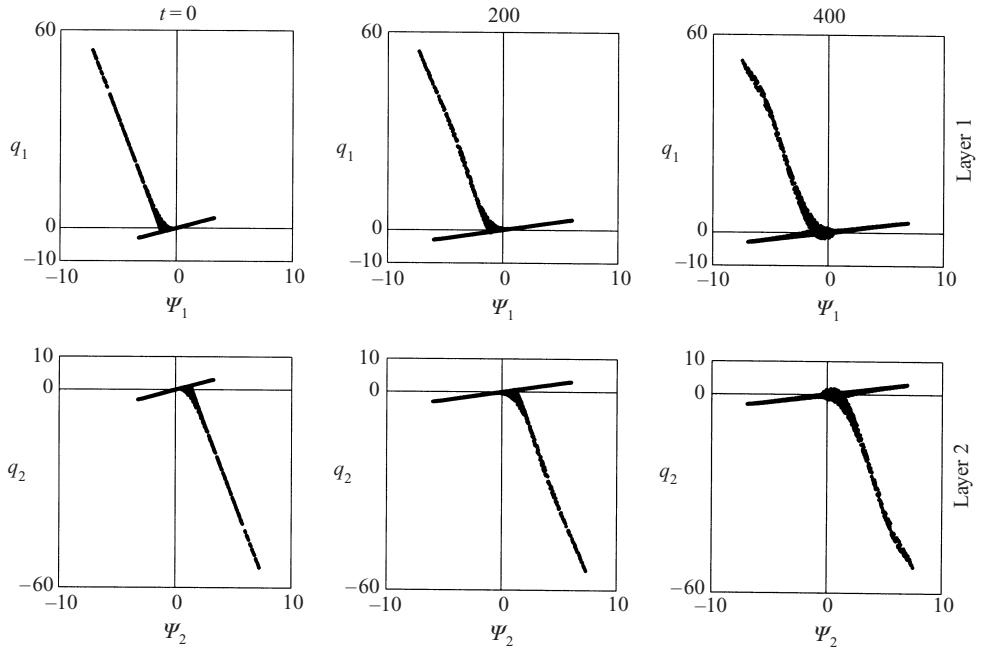

FIGURE 3. PV vs. streamfunction scatters for the layers at $t = 0$, 200, 400 (parameters of the experiment and time units, as in figure 2). The positively sloping straight line, external points; negatively sloping group, internal points.

computed fields, at quasi-steady states it plays the role of a small perturbation acting periodically in time.

4.1.2. *Quasi-stable regimes*

The two plateau phases in figure 2 represent two different quasi-stable regimes. This is evidenced by the well-organized scatter-plots of q_i vs. $\Psi_i (i = 1, 2)$ shown in figure 3. In the first regime, the scatter-plots for the barotropic and the baroclinic modes are also clear-cut and linear (figure 4), i.e. the linear dependencies (11) and (12) hold to a high level of accuracy. This indicates that, in the first quasi-equilibrium state, we are again dealing with a vortex that can be described as a composition of a barotropic Larichev–Reznik dipole and a smooth circularly symmetric rider – a structure given by the solution (7) and (13)–(17). In the second regime, the scatter-plots of q_i vs. Ψ_i are also well grouped; however, they are nonlinear in the trapped-fluid domain (figure 3) and, therefore, the points (q_{BT}, Ψ_{BT}) and (q_{BC}, Ψ_{BC}) are scattered (figure 4). So here we have a vortical structure of a new type.

The streamfunctions and PV in the layers and modes corresponding to the initial state ($t = 0$) and the two quasi-equilibrium states are shown in figures 5–8 (the two moments, $t = 200T$ and $t = 400T$, are chosen as an example). The layer and the barotropic streamfunction fields look qualitatively similar in the two states (figures 5 and 6), the only visible difference being the stronger barotropic dipole component of the second ($t = 400T$). The difference between the two regimes is displayed in the baroclinic mode; it is circularly symmetric in the first state, whereas in the second state it has a saddle-like shape (figures 6 and 8), i.e. when decomposed into a Fourier series in θ, the baroclinic mode contains higher even harmonics ($\cos 2\theta$, etc). Correspondingly, in the first case, the contour demarcating the regions of closed and

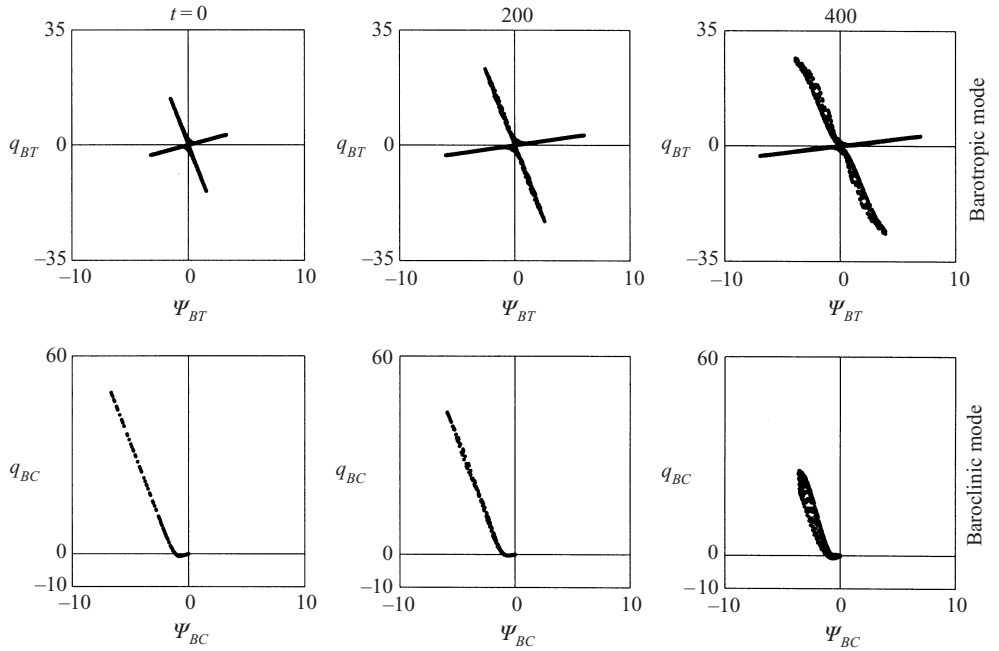

FIGURE 4. PV vs. streamfunction scatters for the barotropic and baroclinic modes at $t = 0$, 200 and 400 (parameters of the experiment, designations and units as in figure 2).

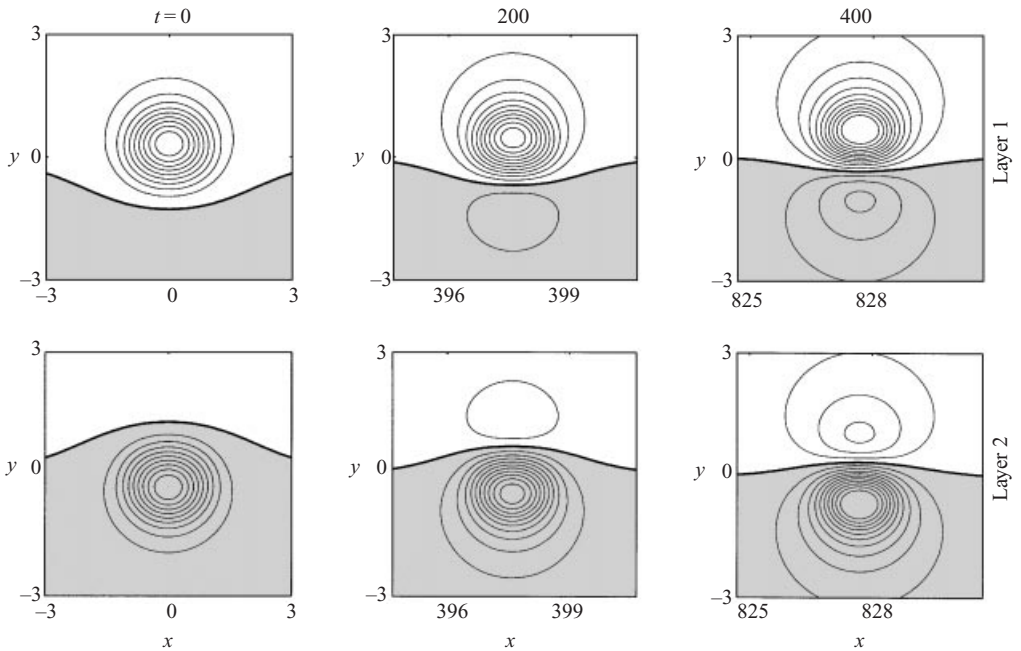

FIGURE 5. Streamfunction fields in the layers at $t = 0$, 200 and 400 (parameters as in figure 2; x and y are given in Rossby radii L_{Ro} time in synoptic periods T). The interval between the contours is 10% of the initial maximum; regions of positive values are shadowed.

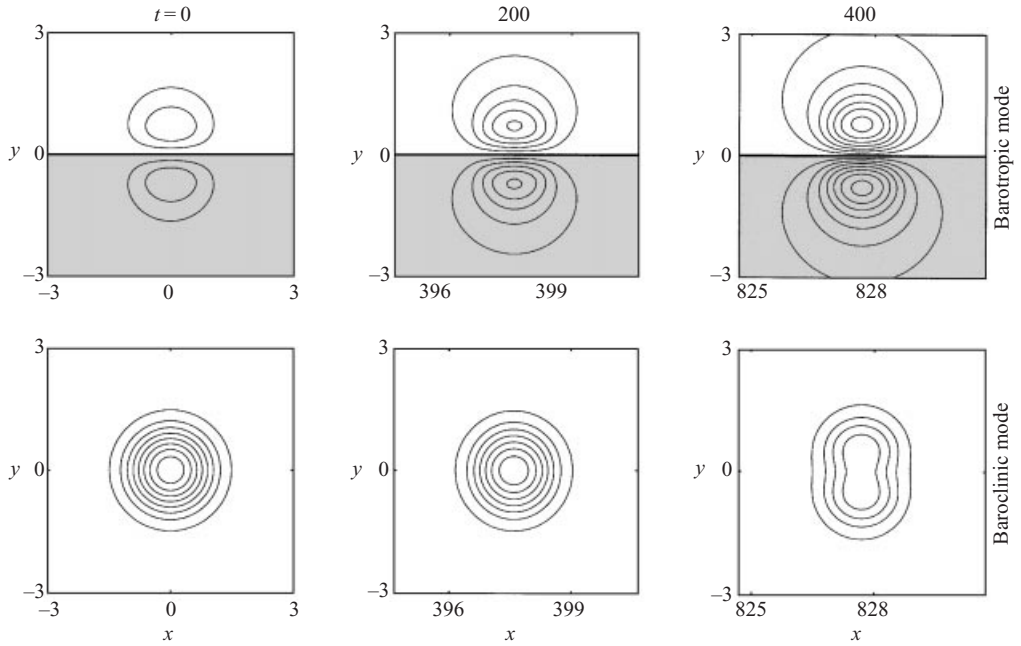

FIGURE 6. Barotropic and baroclinic streamfunction fields at $t = 0$, 200 and 400 (parameters as in figure 2, units as in figure 5). The interval between the contours is 10% of the initial maximum in the layers; regions of positive values are shadowed.

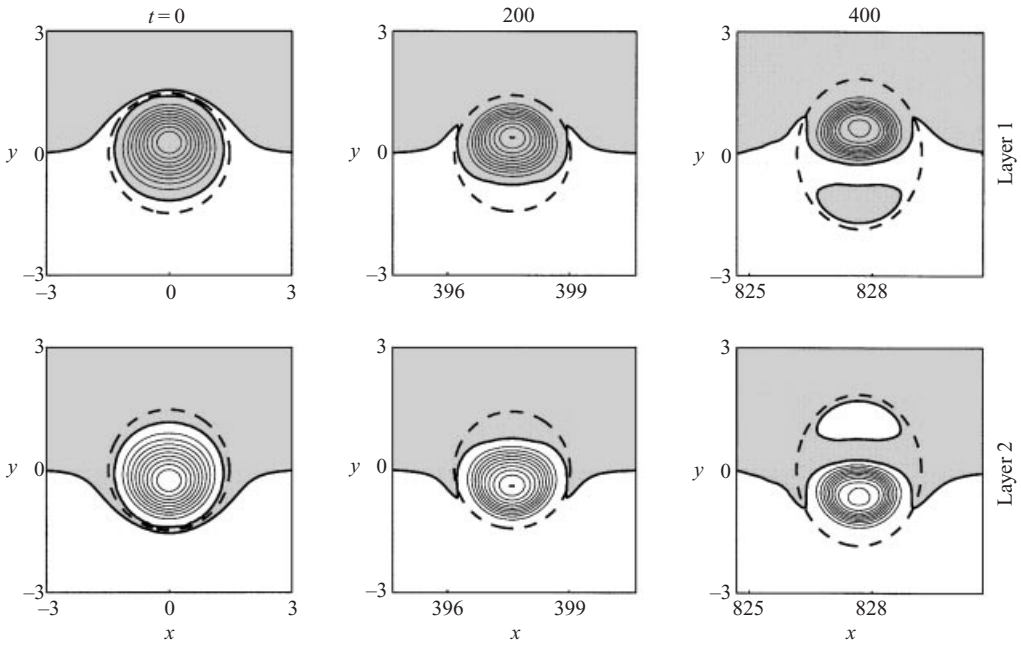

FIGURE 7. PV fields in the layers at $t = 0$, 200 and 400 (parameters as in figure 2; units, contours and shadows as in figure 5). Dashed lines indicate the boundary of the trapped-fluid region.

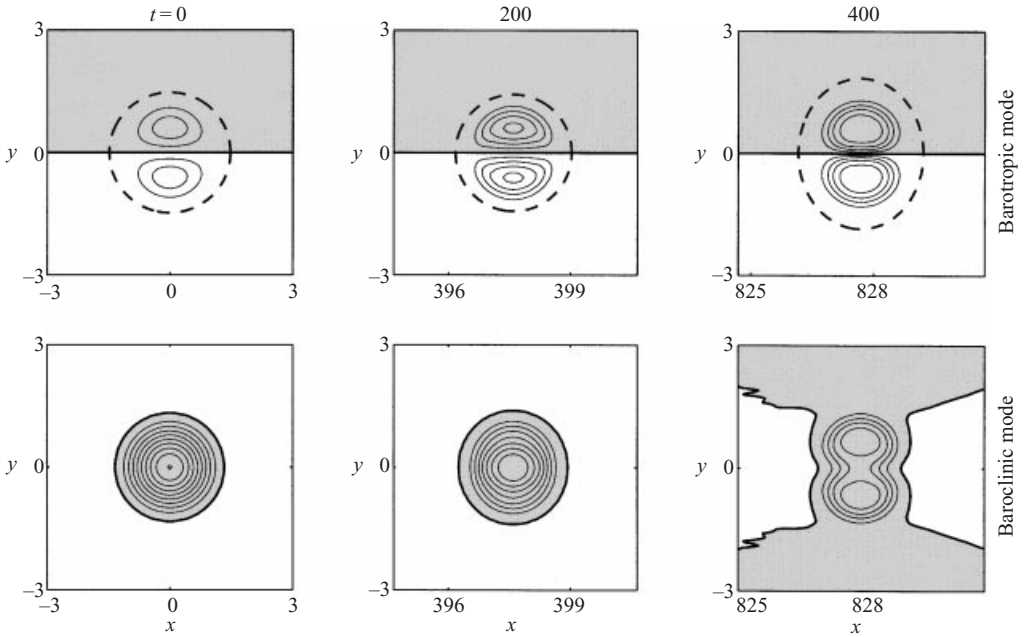

FIGURE 8. Barotropic and baroclinic PV fields at $t = 0$, $200T$ and $400T$ (parameters as in figure 2; units, contours and shadows as in figure 6). Dashed lines indicate the boundary of the trapped-fluid region.

open lines of constant PV is circular, whereas in the second case it is oval in shape (figure 7). We note that in both cases, there is no visible jump in the PV fields when crossing this contour.

As distinct from the circular state, in the oval regime, the distributions of the barotropic and baroclinic PV are quite close in the absolute values (figure 8, $t = 400T$). This means that, within the interior domain, PV in the upper and bottom layers is basically concentrated in different half-planes (with respect to the x-axis). In this sense, the oval modon exhibits a high degree of similarity with a point heton. This regime is even more durable than the circular one: no steep changes in the vortex parameters are observed for at least $1400T$ (until the end of the simulation). We may surmise that this remarkable stability is related to the heton nature of the modon; in hetons, there is a distance at which interaction between the upper and the lower vortices is most intensive and the translation speed is maximal (Hogg & Stommel 1985). Presumably, this distance allows the strongest coupling between the upper and the bottom vortices.

An important question is: do the two quasi-steady configurations described above represent two completely different states or can they be regarded as belonging to the same family? To answer this question, we ran 20 evolutionary experiments at different combinations of the parameters U and A. In most of these experiments a transition of the second type (i.e. from the circular form to an oval state) was observed. The intermediate circular stable regimes differed insignificantly from the initial states if the initial amplitude ratio A_{BC}/A_{BT} ranked approximately from 1 to 1.5, whereas for stronger baroclinic riders, transitions of the first type were also observed. On the other hand, in the cases when the amplitude ratio was small, no sharp transitions were observed; the vortices essentially preserved their initial forms for hundreds of T. The subsequent evolution of these structures was similar to that of the barotropic

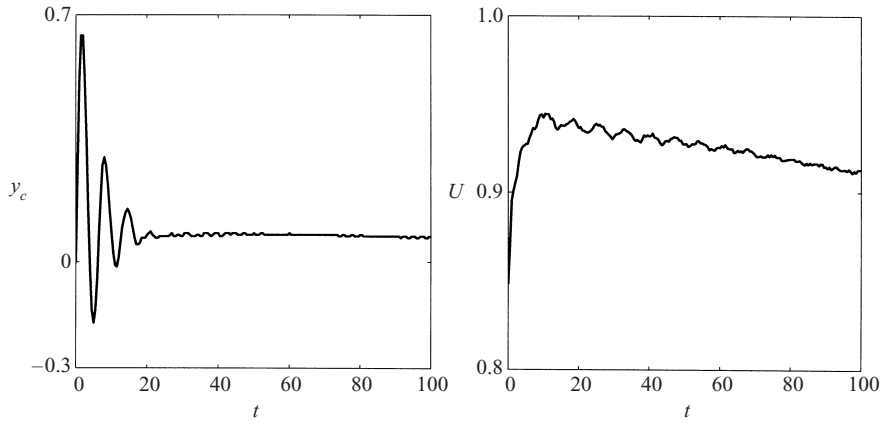

FIGURE 9. Evolution of a tilted modon in the two-layer 'linearly' stratified fluid. Initial state – solution (7), (13) and (17) at $U = 1$ and $A_{BC}/A_{BT} = 1$ turned by 30° with respect to the x-axis: (a) y-coordinate of the vortex centre; (b) x-component of the vortex centre speed (distance in Rossby radii L_{Ro}, speed in L_{Ro}/T).

Larichev–Reznik dipoles: the hindering effect led to slowing down of the eastward drift and, in a long-term perspective, to loss of coherence between the upper and the bottom vortices (which, however, took quite a long time if the initial translation speed was not too small).

Qualitatively, the same main results were obtained in a few experiments in which asymmetric perturbations were imposed on the initial states by tilting the barotropic mode relative to the x-axis. As an example, the initial stage of the evolution of a modon with a moderate rider ($A_{BC}/A_{BT} = 1$) tilted by 30° with respect to the x-axis is presented in figure 9, where the y-coordinate of the vortex centre, y_C, and the x-component of its speed, U, are plotted as functions of time, the centre being defined as the point equidistant from the upper and the bottom streamfunction peaks. This evolution is similar to that of a tilted eastward-propagating barotropic dipole (Nycander 1992; Hesthaven *et al.* 1993): after a few decaying oscillations, approximately at $t = 20T$, the vortex nearly stabilizes in a state close to an exact circular-modon solution. Qualitatively, the further behaviour of the vortex is little different from that of non-tilted circular modons bearing moderate riders; at about $t = 150T$ a transition to an oval state starts.

In the solution (13)–(17), the amplitude coefficient of the baroclinic rider, A, does not affect either the barotropic mode or the structure of the baroclinic mode, so that the smooth circular modons constitute a two-parameter family. A specific solution from amongst this family is determined by the pair (U, A) or, alternatively, (a, A); recall that a and U are related via the dispersion relationship (figure 1). In contrast, the non-smooth circular solutions, in which continuity of q_{BC} at the contour $r = a$ is not required, make up a three-parameter family, the parameters being a, U, and the baroclinic mode amplitude. Similarly, in the general case of non-circular modons, once the form of the trapped-fluid region is fixed up to a homothetic transformation, the corresponding family of non-smooth modon solutions must depend on three parameters: the modon mean size, r_0 (defined as the square root of the trapped-water area); the translation speed, U; and the baroclinic mode amplitude, A_{BC}. Imposing the continuity condition upon the baroclinic PV field will reduce one degree of freedom, resulting in a 'dispersion relationship' between these parameters.

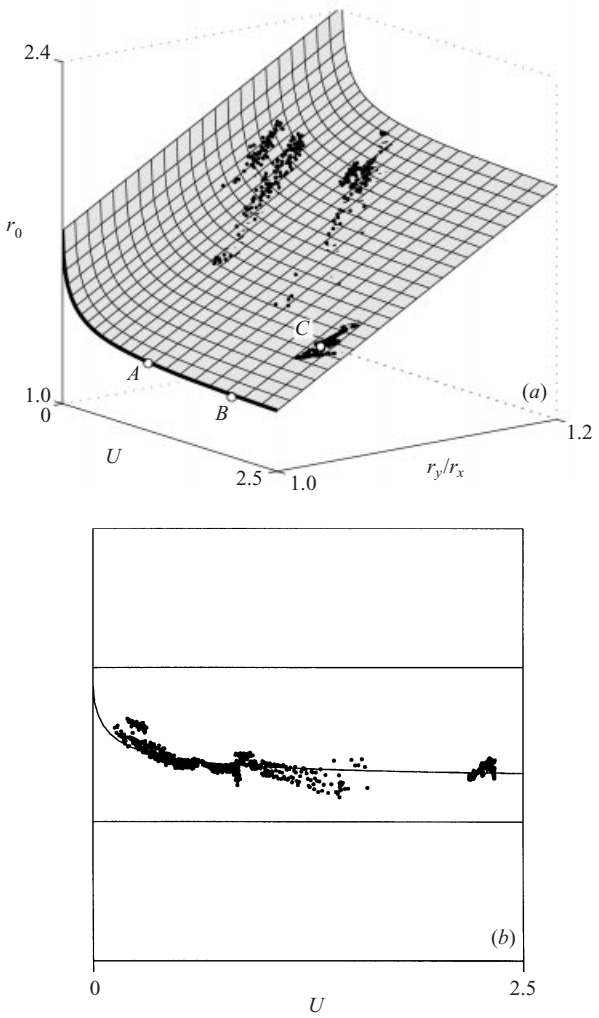

FIGURE 10. Oval quasi-steady states as points in the three-dimensional space (U, r_y/r_x, r_0): (a) three-dimensional image of the experimental points and the fitted cylindrical surface (bold line, directrix $\mathscr{L}$); open circles A, B and C designate the initial state and the two quasi-steady regimes resulted from the transitions; (b) two-dimensional projection in the generatrix direction of the three-dimensional box (shown in (a)) with the experimental points and fitted surface (ordinate, projection of (r_0, r_y/r_x)-plane); for details see § 4.1.2.

Obviously, when a quasi-stationary modon is obtained in a numerical evolutionary experiment, its form is determined only approximately. Nevertheless, in our data, the boundary of the trapped-fluid domain is a convex figure resembling a circle stretched out slightly in the y-direction and, to a first approximation, the ratio r_y/r_x between the large and the small radii can represent this form. Hence, we are dealing here with four parameters r_0, U, A_{BC} and r_y/r_x that, owing to the continuity of the baroclinic PV field, must be related by a 'dispersion relationship' $r_0 = r_0(U, r_y/r_x, A_{BC})$. The latter can be visualized as a family of two-dimensional surfaces or a three-dimensional manifold $\mathscr{M}$ in the three-dimensional space, where the coordinates are r_0, U and r_y/r_x.

One might expect that, in the limit $r_y/r_x \to 1$, smooth oval modons turn into smooth circular modons and, at $r_y/r_x \to 1$, the manifold $\mathscr{M}$ turns into the curve $\mathscr{L}$

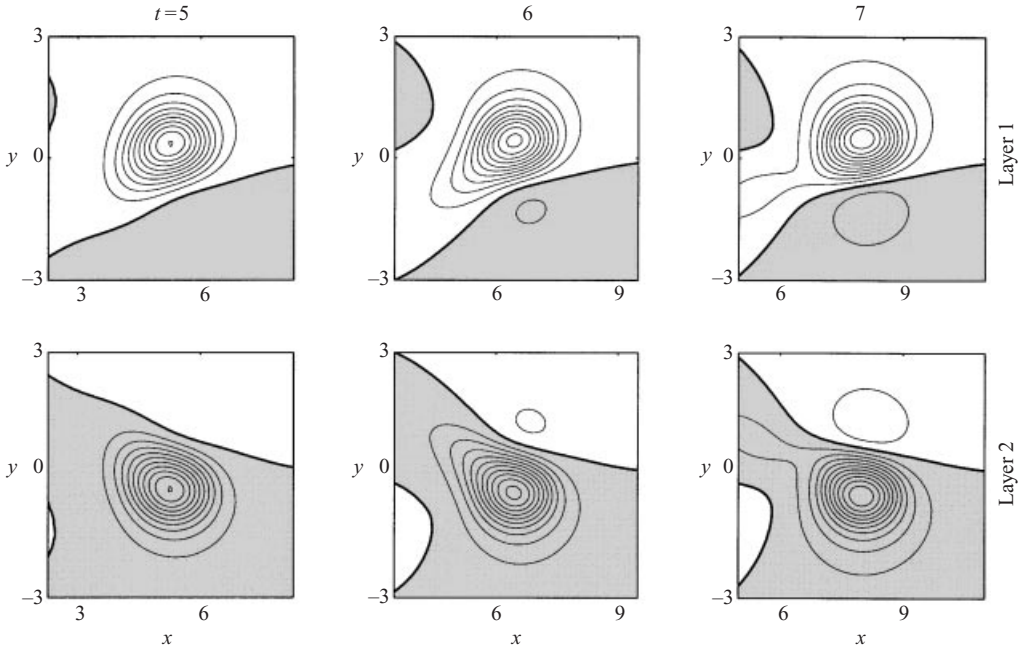

FIGURE 11. Emission of the westward-propagating vortical structure in terms of the streamfunction in the layers (parameters as in figure 2; units, contours and shadows as in figure 5).

representing the lower branch of the dependence $r_0 = r_0(U)$ shown in figure 1. To verify this hypothesis, the oval quasi-steady states obtained in the simulations are plotted as points in a three-dimensional space $(U, r_y/r_x, r_0)$ and a cylindrical surface is fitted to the experimental points so that the curve $\mathscr{L}$ serves the directrix (at $r_y/r_x = 1$), while the generatrix is parallel to the $(r_0, r_y/r_x)$-plane (figure 10*a*). These points form an aggregation in the vicinity of the curve $\mathscr{L}$. (Because, in the quasi-steady stages, the modon parameters varied slowly with time, each experiment is represented by a chain of points.) Inspecting the projection of the aggregation in the generatrix direction proves that it is indeed quite compact (figure 10*b*). In figure 10(*a*), points *A*, *B* and *C*, respectively, indicate the initial state ($t = 0$) and the two modon configurations (at $t = 200T$ and $t = 400T$) achieved in the first and second transitions (base experiment).

4.1.3. *Transitions*

The following analysis of the transition processes is based mainly on the simulation presented in figures 2–8.

The first transition that takes place around $t = 5T$ to $8T$ (figures 11–13), is marked by shedding a considerable amount of PV (figure 12). Transitions of this type were observed only in modons with relatively strong riders ($A_{BC}/A_{BT} > 1.5$), and the stronger the rider, the more sizable was the detached PV patch. In order to understand this phenomenon, we ran two additional experiments in which the initial state was given by the baroclinic mode of the exact solution considered above and, alternatively, by a Gaussian purely baroclinic monopole of a similar shape and strength. The sequence of processes in these experiments was essentially the same as in the basic experiment with the solution (7) and (13)–(17). This suggests that for relatively strong riders, the presence of the barotropic mode and the exact structure

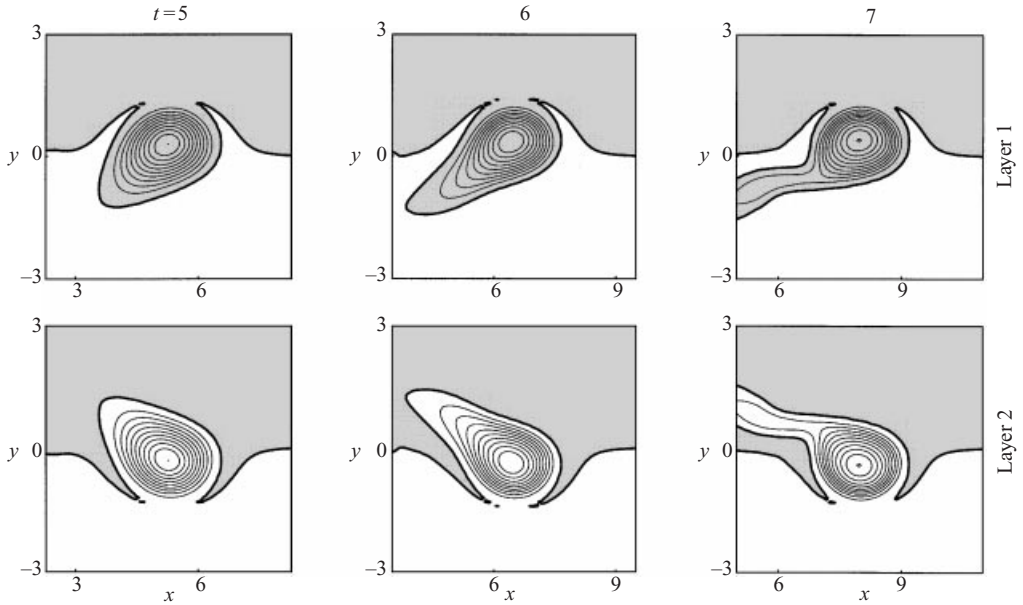

FIGURE 12. Same as in figure 11, but in terms of PV in the layers (contours and shadows as in figure 5.

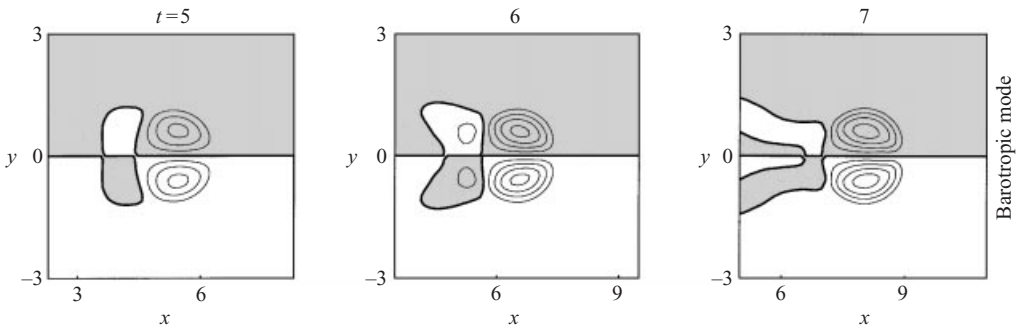

FIGURE 13. Same as in figure 11, but in terms of barotropic PV (contours and shadows as in figure 6).

of the baroclinic mode are immaterial, so that the mechanism of the first transition can be explained in terms of the baroclinic β-gyres.

The notion of baroclinic β-gyres was suggested by Reznik, Grimshaw & Sriskandarajah (1997), who used an asymptotic approach to analyse the evolution of a purely baroclinic two-layer 'linearly' stratified monopole. These are high-order dipolar and antisymmetric about the y-axis corrections to the circular current in each layer that develop at an early stage of the evolution of a baroclinic monopole and pull apart the upper and the bottom monopoles thus forming a zonally propagating heton. In both layers, the main (circular) currents and the eastern halves of the β-gyre corrections are opposite in sign. Therefore the eastern periphery of the vortical system becomes somewhat depressed; for a similar reason, the western periphery is strengthened. Thus, the vortices in the upper and the bottom layers elongate in the westward direction (figures 11 and 12). Since the main (zero-order) currents in each of the layers advect the baroclinic β-gyres, one of them turns clockwise and the other counterclockwise.

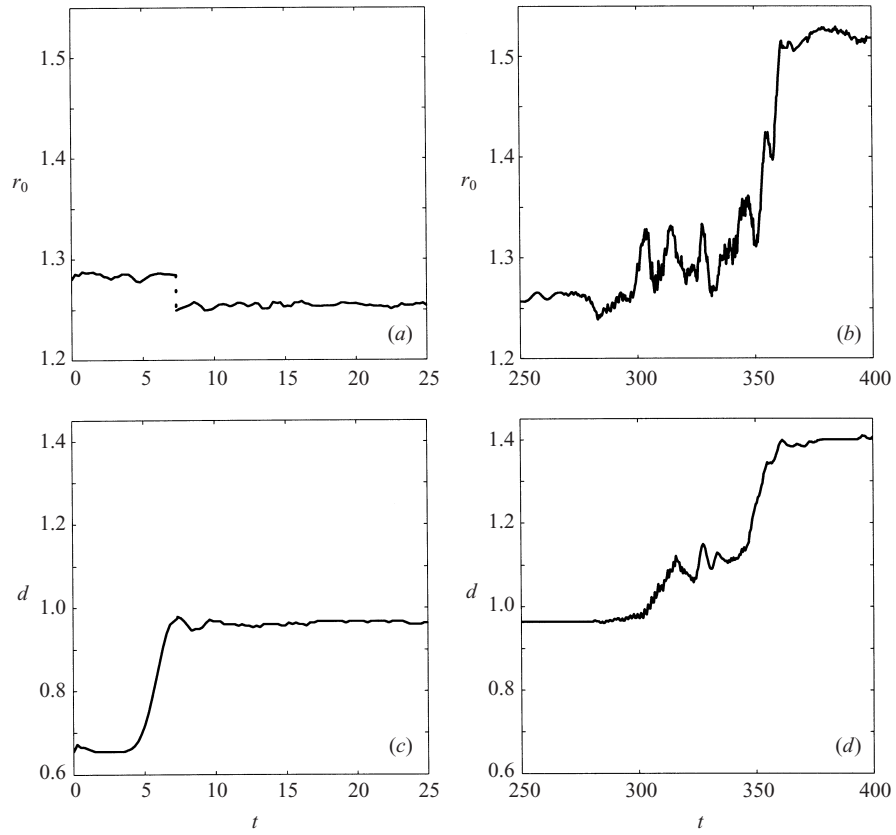

FIGURE 14. (a, c) The first, and (b, d) the second transitions (parameters as in figure 2): (a, b) average radius of the trapped-fluid area; (c, d) distance between the streamfunction poles in the upper and bottom layers. Time is given in synoptic periods T; mean radius and distance in Rossby radii L_{Ro}.

Consequently, the rear (elongated) parts of the upper and the lower vortices overlap and start working as a westward-travelling heton. In the barotropic PV field, it is embodied in the creation of a relatively weak dipole, negative in its northern half and positive in its southern half (figure 13). This process leads to the separation of the stronger forward (right-hand), and the weaker rear (left-hand) vortical structures at about $7.3T$, the westward vortex being surrounded with a nonlinear Rossby-wave field (cf. Kizner & Berson 2000). (Note that formally, because of the PV conservation that forbids the breaking and closing of PV contours (e.g. Larichev 1983*a*, *b*), the separated vortices must be connected by some filaments. However, these filaments may thin down so that no grid numerical model will be able to resolve them.)

This transition was monitored by calculating the average radius r_0 of the trapped-fluid domain estimated as the square root of the area of closed PV contours in one of the layers, and of the distance d between the streamfunction poles in the upper and bottom layers (figure 14). After the separation, within the period $t = 7.3T$ to $10T$, the remaining eastward vortex structure reorganizes into a circular modon composed of a dipolar barotropic mode symmetric about the y-axis, and a baroclinic circularly symmetric rider. The small oscillations in r_0 and d (figures 14*a* and 14*c*) attending the first transition have a period approximately $1T$ and die out gradually by about $t = 20T$, when all the modon parameters stabilize. The shedding of the westward vortex results in the radius of the modon under consideration being smaller than that

of the vortical structure before the separation. The estimated U and r_0 satisfy the dispersion relationship for circular modons (equations (16) and (17); figure 1) to a high degree of accuracy. Accordingly, in spite of the contraction of the trapped-fluid domain (as compared to its initial size), the barotropic dipole becomes stronger and the vortex gains a higher translation speed. The weakening of the baroclinic mode and strengthening of the barotropic mode (figure 2*c*) show up also in the increase of the distance d between the poles of ψ_1 and ψ_2 (figure 14*c*).

Naturally, the analogy between the evolution of a circular modon and that of a baroclinic monopole (used to explain the mechanism of shedding vorticity patches by the modon) is legitimate if the baroclinic rider is sufficiently strong. The case for the use of this analogy in the analysis of our runs is that transitions of the first type occurred only when the baroclinic-to-barotropic amplitude ratio exceeded 1.5.

The second transition lasts approximately from $t = 280T$ to $370T$. During this period, the translation speed increases again (figure 2*d*), and thereafter the vortical structure stabilizers in a new, non-circular state, in which the trapped-fluid area is oval in form (figures 7, 8). In figures 14(*b*) and 14(*d*) we can see an upward trend superimposed by two oscillatory processes (those characterized by the periods of about $1T$ and $10T$). While oscillating, the vortex deforms the surrounding vorticity field and draws into rotation the neighbouring fluid. Therefore, along with the detachment of filaments, an entrainment of external fluid particles by the vortex can be observed (figure 15). According to our data, the entrainment has a stronger net effect resulting in growth of the trapped-fluid area (figure 12*b*).

In all likelihood, the perturbing factor that triggers the transition of the vortex structure from a circular to an oval state is the accumulated numerical hindering effect – the delay in the eastward translation (figure 2*d*). It gradually destroys the relationship (16)–(17) between the modon radius and the translation speed (i.e. the balance between the barotropic and the baroclinic components of the movement) causing oscillations of the upper and the bottom vortices (figures 14*b* and 14*d*). Because the high-frequency oscillations start first, we may speculate that they induce the stronger lower-frequency oscillations. When the perturbations reach a certain critical level, the vortex undergoes a relatively sharp transition (figures 14*b* and 14*d*; time period from $350T$ to $370T$). In the transition stage, the vortex structure increases its mean radius, and the potential energy (that, coupled with the baroclinic mode) is used to strengthen the barotropic mode. The whole structure accelerates, while the upper and the lower vortices tend to drift apart (figures 2*d* and 14*d*).

We note that, in the context of PV conservation, we can speak only of neutral stability. In other words, being subjected to small but uninterrupted perturbations, a vortex that would otherwise be steady may change its parameters, while 'creeping' along the manifold of stationary (quasi-stationary) states. If so, what causes the circular modon to leap rapidly to a relatively remote oval state instead of passing through a sequence of quasi-stable states, thus evolving slowly? We believe that the answer is related to the invariants of the experiment. It is true that, owing to the finite-difference approximation and the cutting applied, some of the characteristics that, theoretically, should be conserved, may vary during a simulation. However, because the main events of the second transition move in the neighbourhood of the vortical core (see, for example, figure 15), the total energy in the box $[-X < x < X;\ -Y < y < Y]$ barely changes, while the total enstrophy drops by 2%; the peak PV values also remain nearly constant. Thus, in the state to which the modon changes, the values of the above characteristics must be close to those before the transition started. Such an oval state may be distant from the circular state in terms of r_0, U

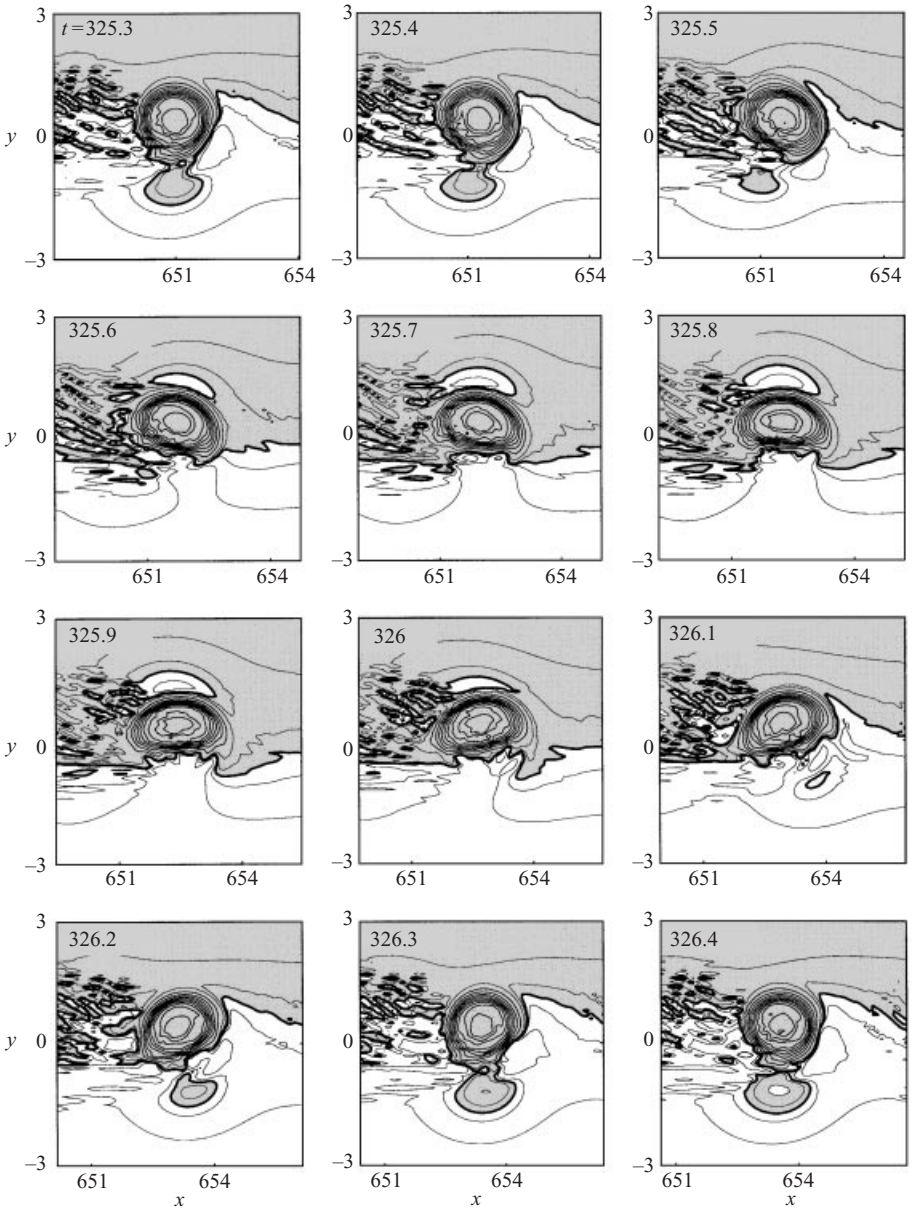

FIGURE 15. The upper-layer PV field in the second transition (parameters as in figure 2; units and shadows as in figure 6; the contour intervals are: 1, 3 and 10% of the initial maximum).

and r_y/r_x. This reasoning is supported by a check simulation, in which the cutting is turned off at $t = 280T$; its results are quite close to those obtained in the basic experiment.

4.1.4. *Sharp stratification*

Along with the experiments described above, in which the unperturbed depths of the fluid layers were equal, experiments with the solution (7) and (13)–(17) at the ratio $h_1 : h_2 = 1 : 4$ (the case of 'sharp' stratification) were run. These experiments are beyond

the scope of the present publication. One of them, however, is worth mentioning here (see also § 4.2.1); we found that, at a moderate translation speed, $U = 0.25$, and quite a large rider-to-dipole amplitude ratio ($A_{BC}/A_{BT} = 3$), the initial configuration can be preserved for about $200T$. This suggests that stable configurations of the circular type with relatively strong baroclinic riders can exist in a sharply stratified fluid.

4.2. *Three-layer modons*

We will confine ourselves to the case where the density jumps between the layers are equal and the upper and the lower layers are of the same thickness, i.e. $h_1 = h_3 = h$; the mid-layer depth remains unspecified for the present. By denoting

$$\varepsilon = \frac{h_1 + h_3}{h_2} = \frac{2h}{h_2}, \tag{20}$$

the vertical normal modes in such a model are given by the vectors

$$F^{(0)} = \begin{pmatrix} 1 \\ 1 \\ 1 \end{pmatrix}, \quad F^{(1)} = \begin{pmatrix} 1 \\ 0 \\ -1 \end{pmatrix}, \quad F^{(2)} = \begin{pmatrix} 1 \\ -\varepsilon \\ 1 \end{pmatrix}. \tag{21}$$

Putting $n = 3$ in (5), and substituting (5) and (21) into (1) we obtain the following equations describing the evolution of the barotropic and the baroclinic modes:

$$\frac{\partial}{\partial t} q^{(0)} + J(\psi^{(0)}, q^{(0)}) + \frac{\varepsilon}{1+\varepsilon} J(\psi^{(1)}, q^{(1)}) + \varepsilon J(\psi^{(2)}, q^{(2)}) = 0, \tag{22}$$

$$\frac{\partial}{\partial t} q^{(1)} + J(\psi^{(0)}, q^{(1)}) + J(\psi^{(1)}, q^{(0)}) + J(\psi^{(1)}, q^{(2)}) + J(\psi^{(2)}, q^{(1)}) = 0, \tag{23}$$

$$\frac{\partial}{\partial t} q^{(2)} + J(\psi^{(0)}, q^{(2)}) + J(\psi^{(2)}, q^{(0)}) + \frac{1}{1+\varepsilon} J(\psi^{(1)}, q^{(1)}) + (1-\varepsilon) J(\psi^{(2)}, q^{(2)}) = 0. \tag{24}$$

There are two ways to fit a solution of the type (7) and (13)–(17) to a three-layer stratification; the rider can be associated with either the first or the second baroclinic mode. We will consider both of these cases, starting with the second.

4.2.1. *Modon with a rider in the second baroclinic mode*

As seen from equation (23), if at $t = 0$ the first baroclinic mode is zero, it remains zero for any t. Equation (23) then becomes trivial ($q^{(1)} \equiv 0, \psi^{(1)} \equiv 0$), whereas by introducing the notations

$$\psi^{(0)} = \psi_{BT}, \quad \psi^{(2)} = \psi_{BC}, \tag{25}$$

equations (22) and (24) are immediately reduced to (18) and (19). Equations (8) in the two-layer model ($j_0 = 1$) and the three-layer model ($j_0 = 2$) are also identical as in the two cases $m_{j_0}^2 = (f_0^2/g'h_1)(1+\varepsilon)$, where $g' = g(\delta\rho/\rho_0)$ is reduced gravity, while ρ_0 and $\delta\rho$ are the mean density and density jump, respectively. Thus, the evolution of a three-layer vortex given by the solution (7), (13)–(17) and (25) can be considered in terms of the two-layer dynamics. (In a manner similar to the two-layer case, equations (22) and (24) at $\varepsilon = 1$ also describe the evolution of the zero and the second modes in a continuously and linearly stratified fluid in the three-mode approximation on condition that, at $t = 0$, the first baroclinic mode is zero and the vertical normal modes are normalized so that $F^{(0)} = 1$, $F^{(2)}(0) = \sqrt{2}$.)

The analogy between the two-layer and three-layer models in the absence of the first baroclinic mode is quite natural. Indeed, in this case, the vortices in the upper

and bottom layers of the three-layer fluid are identical. Consequently, the upper and lower layers perturb the middle layer identically, and their combined effect upon the middle layer can be interpreted in terms of a two-layer model as the influence of one layer of a non-perturbed depth $2h$ upon the other layer, whose depth is ε. There is, however, some specificity in this analogy. For example, the case of the three-layer 'linear' stratification ($h_1 = h_2 = h_3$), in which $\varepsilon = 2$, corresponds to a two-layer model, in which the stratification is taken as $h_1 : h_2 = 2:1$. If we interchange the indices of the layers in the two-layer model, it will be seen that this case is also equivalent to the case $h_1 : h_2 = 1:2$. Hence, both high and low values of ε determine, in essence, the same dynamics typical of 'sharp' stratification (see § 4.1.4). On the other hand, the two-layer 'linearly' stratified model ($h_1 : h_2 = 1:1$) corresponds to a three-layer model, in which the middle layer is twice as thick as each of the other layers ($h_1 : h_2 : h_3 = 1:2:1$). In such a three-layer model, $\varepsilon = 1$. This relationship between $h_1 = h_3$ and h_2 is the only one that guarantees the conservation of the symmetry and antisymmetry about the x-axis of the baroclinic and the barotropic mode, respectively.

All the conclusions regarding the evolution of the circular two-layer modons can now be applied to the three-layer vortices (taking into account the relationships between the layer depths that allow the analogy). In particular, if $\varepsilon = 1$, transitions from the circular to oval states are possible. On the other hand, robust circular modons can also exist when the three-layer stratification is sharp (§ 4.1.4).

According to (20) and (21), the thinner the middle layer in the three-layer model, the larger the value of ε, and the larger the contribution of the second baroclinic mode to the mid-layer motion; it exceeds that of the second baroclinic mode to the upper and the lower layers if $\varepsilon > 1$ (i.e. $h_2 < 2h$). Consider now, for example, a three-layer fluid, in which $h_1 : h_2 : h_3 = 2:1:2$, i.e. $\varepsilon = 4$. Let us next assume that the rider amplitude in the first layer is three times larger than the amplitude of the barotropic mode, and the translation speed is equal to 0.25. Such a modon will be situated in the middle layer, where its baroclinic rider will be 12 times stronger than the baroclinic dipole. A modon of this type can be interpreted as an eastward-travelling intrathermocline oceanic vortex (cf. Kizner 1984*b*). Taking into account the equivalence of the two types of stratification in the two-layer model – those at $\varepsilon = 0.25$ and $\varepsilon = 4$, we arrive at the conclusion that this three-layer construction will behave in exactly the same persistent manner as the two-layer vortex (at $h_1 : h_2 = 1:4$) considered above (§ 4.1.4).

Although most of the intrathermocline lenses observed in the ocean have a westward component in their drift (e.g. Kamenkovich *et al.* 1986, chap. 5), the eastward-going lenses can exist. In the numerical experiments on the evolution of the intrathermocline Mediterranean Water eddies (meddies), performed by Morel & McWilliams (1997) in the quasi-geostrophic model with high vertical resolution, intrathermocline vortices, translating steadily eastward, emerged. The emerged vortex had a strong axisymmetric baroclinic component and a dipolar barotropic component.

4.2.2. *Modon with a rider in the first baroclinic mode*

Let us now consider the evolution of a three-layer vortex given by the solution (7) and (13)–(17), in which the rider is associated with the first baroclinic mode:

$$\psi^{(0)} = \psi_{BT}, \quad \psi^{(1)} = \psi_{BC}. \tag{26}$$

The presence of the term $J(\psi^{(1)}, q^{(1)})$ in (24) allows the development of the second baroclinic mode even though it is absent in the initial state. Therefore, in contrast with the previous case (§ 4.2.1), numerical simulations are required to study the properties of such dipole-plus-rider structures. The symmetry/antisymmetry of the

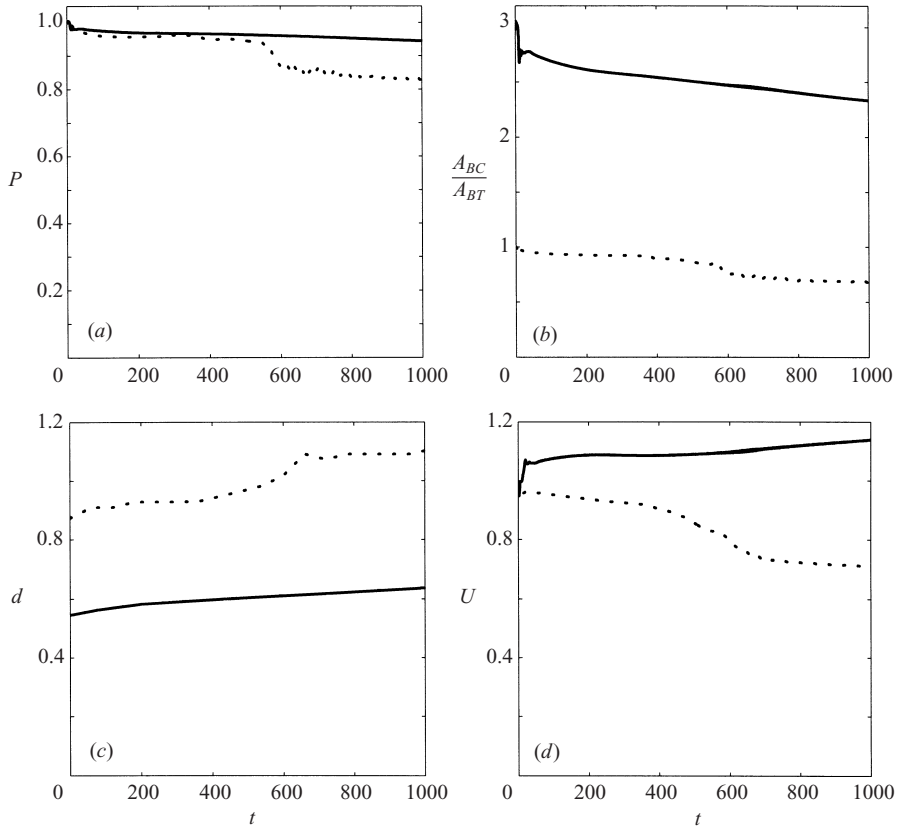

FIGURE 16. Evolution of a modon in the three-layer 'linearly' stratified fluid; the initial state is given by equations (7) and (13)–(17) at $U = 1$ with the rider in the first baroclinic mode: ——, $A_{BC}/A_{BT} = 3$; - - -, $A_{BC}/A_{BT} = 1$. (*a*) Total potential energy normalized with the initial value; (*b*) baroclinic-to-barotropic amplitude ratio; (*c*) distance between streamfunction poles in the middle layer; (*d*) translation speed (units as in figures 2 and 9).

modes, however, can be judged directly from equations (22)–(24). According to (24), if the second baroclinic mode started developing, it would be antisymmetric about the x-axis. Correspondingly, as seen from (22) and (23), the barotropic mode will remain antisymmetric and the first baroclinic mode will remain symmetric about the x-axis.

We performed numerical experiments for the particular case of a three-layer 'linear' stratification, $h_1 = h_2 = h_3$, initializing the model by the solution (7), (13)–(17) and (26) at the translation speed $U = 1$ and the radius $a \approx 1.03$ (which corresponds to the unit translation speed at such a stratification). The experiments lasted up to $t = 1000T$.

The first experiment was carried out for the case $A_{BC}/A_{BT} = 1$ (figures 16–18). In this run, the total potential energy remains practically constant by $t \approx 550T$, when a mild transition starts (figure 16*a*). This transition separates two quasi-steady phases, which are apparent also in the graphs of the baroclinic-to-barotropic amplitude ratio (figure 16*b*), distance d between the poles of ψ_2 (figure 16*c*), and the translation speed U (figure 16*d*). The differences between these phases are hardly visible in the upper and bottom layers (figure 17), but the analysis of the modal components of the streamfunction reveals that in the first phase the vortex remains essentially the same as at the onset of the simulation, whereas in the second, it is an oval structure

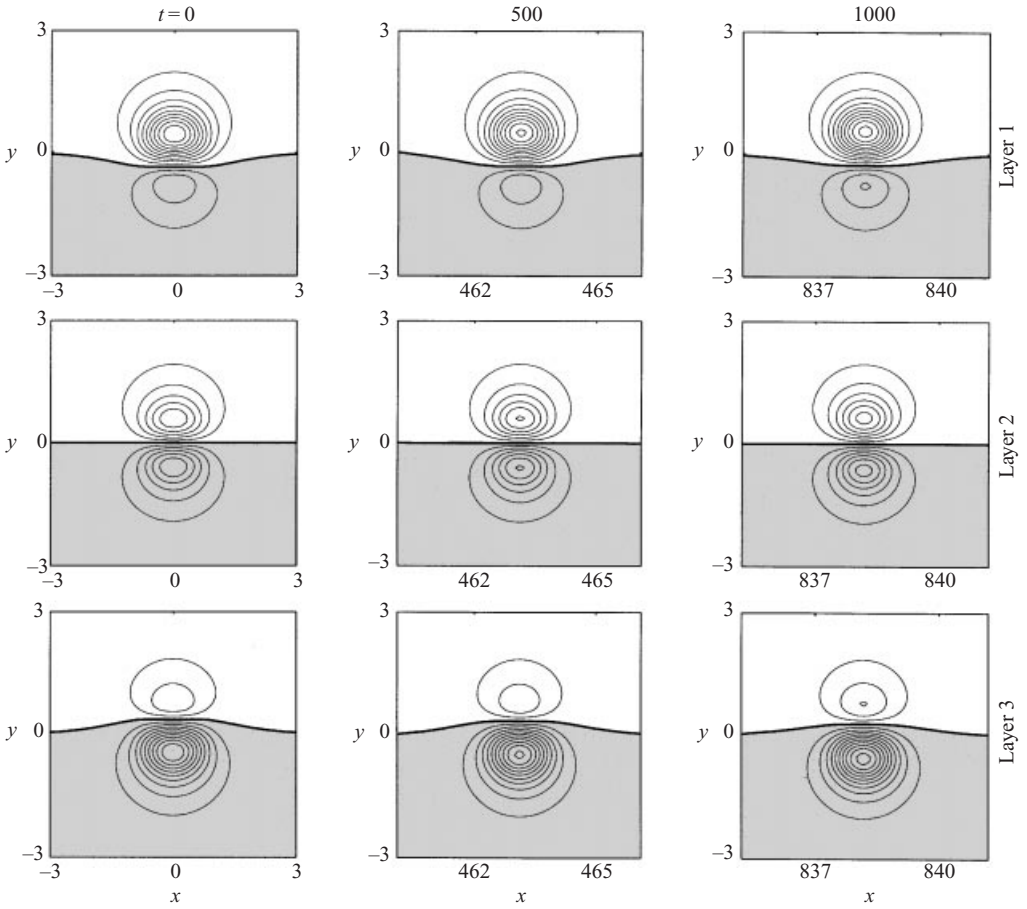

FIGURE 17. Streamfunction fields in the layers at $t = 0$, 500 and 1000. The initial amplitude ratio is 1:1; other parameters as in figure 16 (designations as in figure 5).

(figure 18). The main result of this experiment is that the second baroclinic mode does not actually develop; at $t = 1000T$ it is within the limit of 3% of the maximum in the layers in terms of both the streamfunction and PV. Correspondingly, the vortex in the middle layer is represented by the barotropic mode only (figures 17 and 18).

During the transition, the barotropic dipole becomes stronger at the expense of the weakening baroclinic rider (figures 16*b* and 18). In other words, the potential energy, which is associated here with the first baroclinic mode (the second-mode contribution is negligible), is transferred to the kinetic energy of the barotropic mode. The distance between the halves of the dipolar vortex in the middle layer increases (figure 16*c*), as does the distance between the vortices in the upper and the lower layers. This is manifested in some 'stretching' of the first baroclinic mode in the y-direction (figure 18, $t = 1000T$). As a result, the mutual advection of the vortices in all the layers weakens, and the entire structure slows down (figure 16*d*).

Although some strengthening of the dipole and stretching of the rider takes place before the transition (figure 18, $t = 500T$), those two processes are very weak. By $t = 500T$, the PV *vs.* streamfunction scatter-plots for the layers, the barotropic and the first baroclinic modes are very well organized and close to those for the initial state. After the transition, the trapped-fluid area becomes slightly oval in shape and,

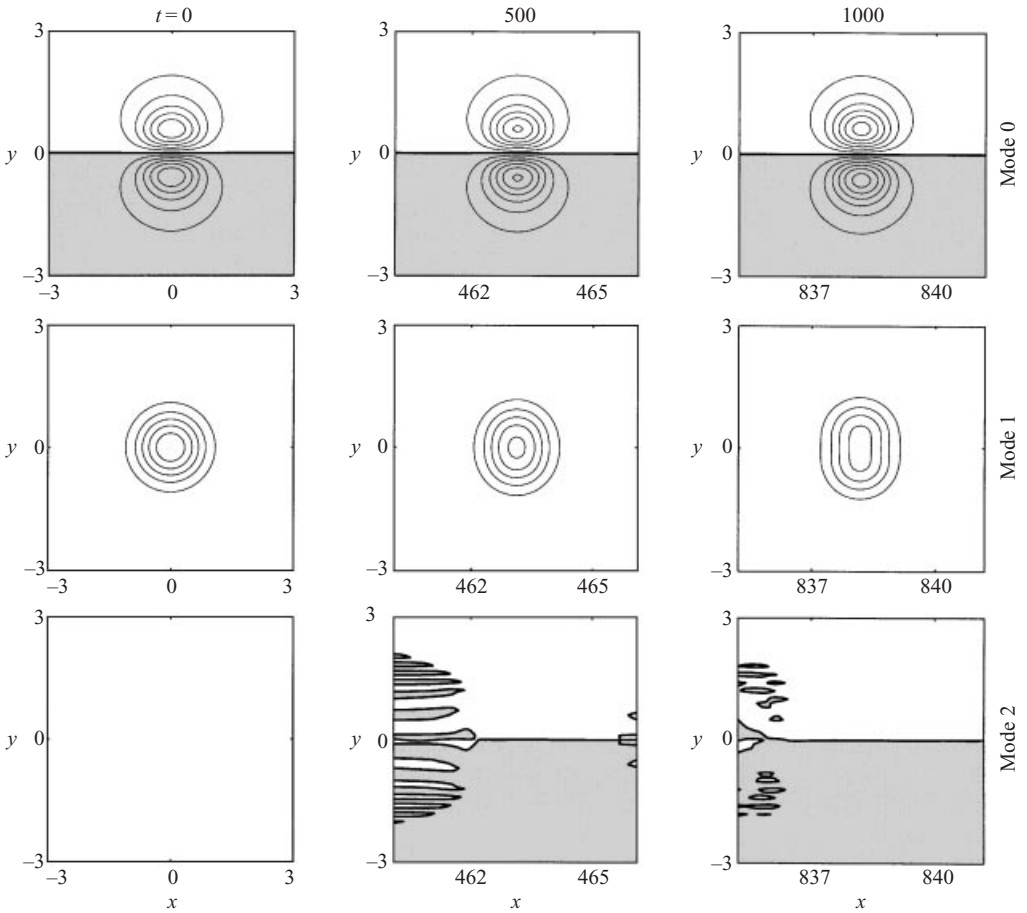

FIGURE 18. Barotropic and baroclinic streamfunction fields at $t = 0$, 500 and 1000. The initial amplitude ratio is 1:1; other parameters as in figure 16 (designations as in figure 6).

correspondingly, the relationship between the PV and the streamfunction in the layers becomes nonlinear.

The results we obtained in the two-layer model (§4.1) suggest that the initial strength of the rider in the above-mentioned experiment was insufficient for the transition of the first type to take place. Therefore, in order to be able to perform a complete comparison of the two- and three-layer simulations, we carried out another evolutionary experiment, in which the initial amplitude ratio was $A_{BC}/A_{BT} = 3$. Here, by $t = 10T$, the vortex makes a short-range transition to a state characterized by a somewhat smaller amplitude ratio and a higher translation speed (figures 16*b* and 16*d*). According to our diagnostics, this state is very well described by the solution (7), (13)–(17) and (26).

The main result of this run is that the vortex barely changed during the computations (figures 19–22). In the course of the quasi-steady eastward drift of the newly formed circular modon, no significant second baroclinic mode is developed (figure 20), so that the extremely slow decrease of the potential energy (figure 16*a*) is reflected only in a slow increase in the kinetic energy of the barotropic mode. This increase, in turn, manifests itself in some strengthening of the barotropic dipole (figure 20) and in

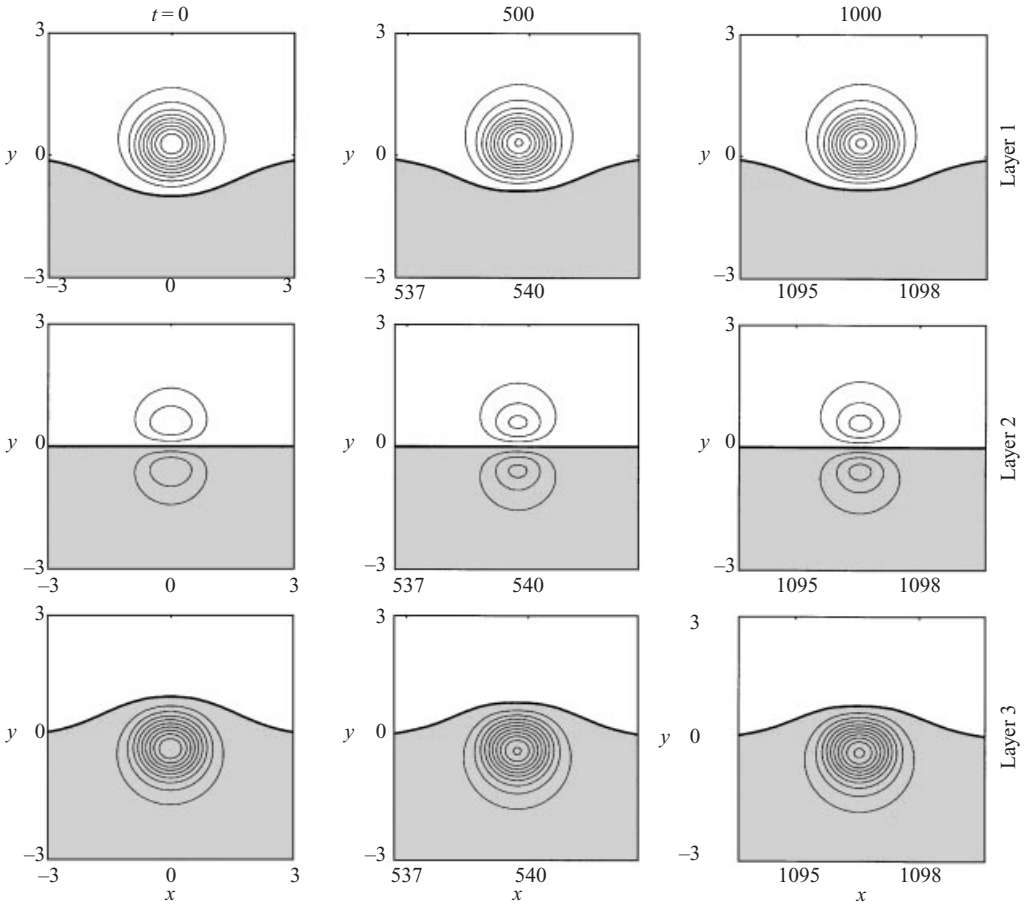

FIGURE 19. Streamfunction fields in the layers at $t = 0$, 500 and 1000. The initial amplitude ratio is 3:1; other parameters as in figure 16 (designations as in figure 5).

a very slow speeding up of the modon (figure 16*d*). Correspondingly, the mid-layer streamfunction and PV fields undergo a very smooth evolution, whereas the changes in the upper and the bottom layers are hardly detectable (figures 19 and 21); the scatter-plots also remain practically the same during the experiment. Thus, evolving slightly, the vortex essentially remains a circular modon (figures 20 and 22, mode 1).

A comparison of these results with those obtained in the two-layer model leads us to believe that the larger the number of layers, the more durable are the modons bearing sufficiently strong riders ($A_{BC}/A_{BT} \sim 3$) in the first baroclinic mode. Consequently, these results can be treated as indirect evidence that, in a continuously (and linearly) stratified fluid, the solution (7) and (13)–(17) represents quite stable vortical structures.

5. Conclusion

We studied numerically the stability properties and the evolution of smooth circular dipole-plus-rider structures in which the boundary of the trapped-fluid area is a circular cylinder and, within this area, the PV depends linearly on the streamfunction. Modons of this type represent exact solutions for both continuously stratified and multi-layer quasi-geostrophic models. Two- and three-layer evolutionary experiments

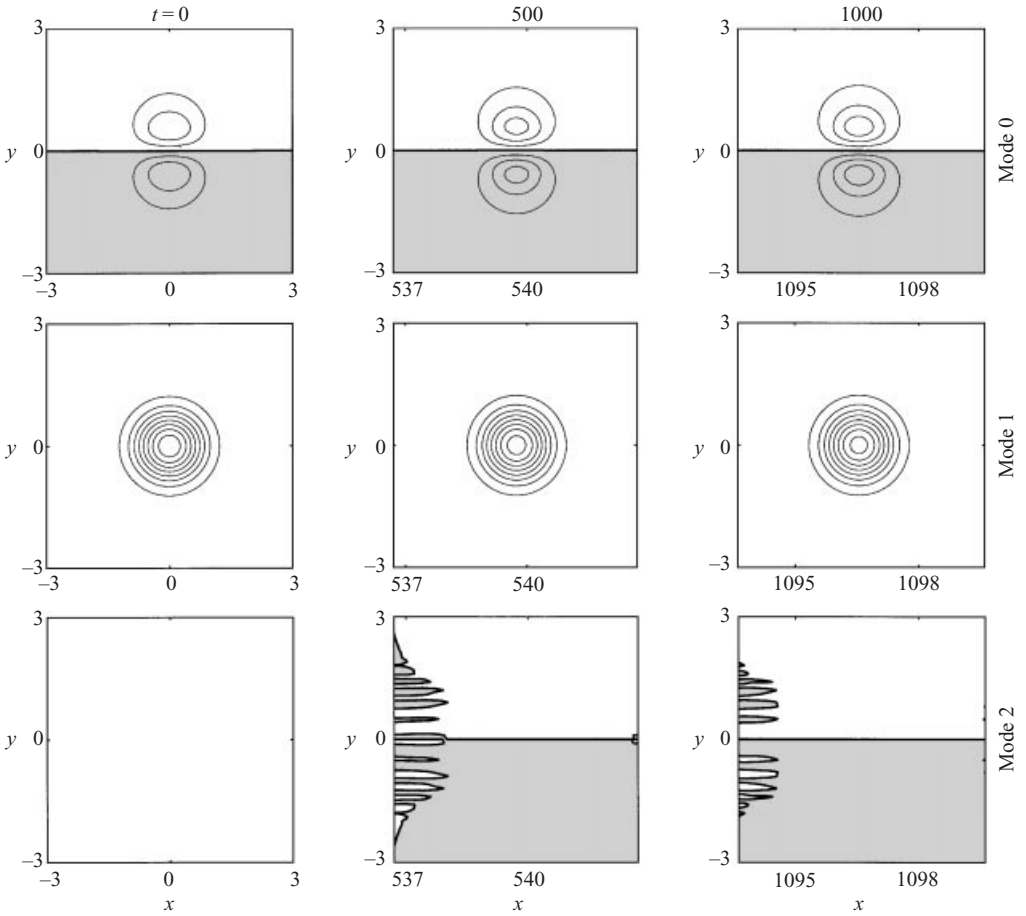

FIGURE 20. Barotropic and baroclinic streamfunction fields at $t = 0$, 500 and 1000. The initial amplitude ratio is 3:1; other parameters as in figure 16 (designations as in figure 6).

were run at different combinations of the free parameters (ratio between the layer depths, translation speed of the modon, and the rider amplitude), the case of equal layer depths ('linear' stratification) being considered in detail.

In a two-layer fluid, when the amplitudes of the baroclinic and the barotropic modes are close to each other and the layers are of the same depth, the vortex displays a stable behaviour for hundreds of synoptic periods. Strengthening of the baroclinic rider leads to the shedding of an amount of PV and a fast transition of the vortex to a new quasi-steady state identified as a circular dipole-plus-rider modon of a smaller radius and a higher translation speed. This newly formed modon travels eastwards quasi-steadily for hundreds of synoptic periods. Even when the forward integration is started from a sufficiently strong purely baroclinic axially symmetric vortex, the latter rapidly transforms into a durable circular modon. This conclusion endorses the results of Flierl & McWilliams (1979) and Mied & Lindemann (1982), who considered relatively short times (tens of T), and those of Pakyari & Nycander (1996), who conjectured that the eastward-travelling baroclinic dipole-plus-rider structures could be stable.

In many runs, the circular steady-state phase is followed by another transition resulting from the numerical hindering of the modon. This transition is somewhat

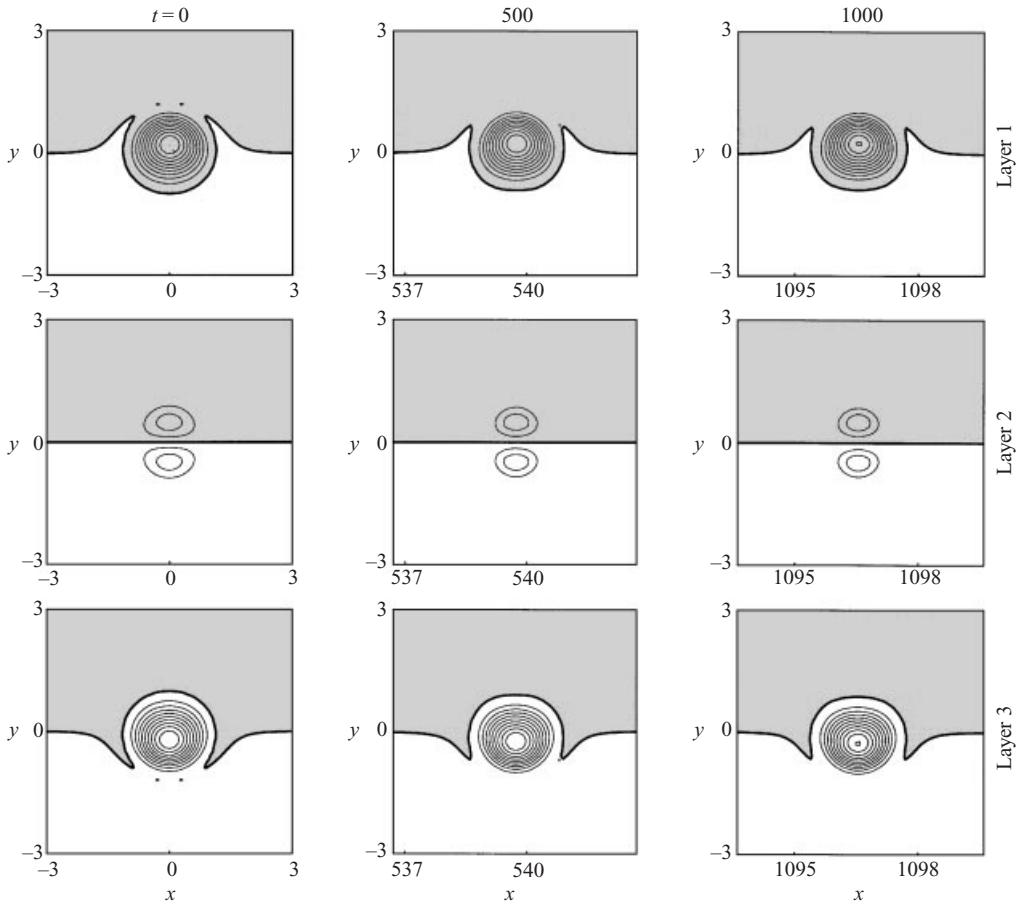

FIGURE 21. PV fields in the layers at $t = 0$, 500 and 1000. The initial amplitude ratio is 3:1; other parameters as in figure 16 (designations as in figure 5).

smoother than the first one and brings the vortex to an oval quasi-steady regime that is even more durable than the circular one; in this state, a modon persists for more than 1000 synoptic periods. In such a state, the PV *vs.* streamfunction dependence in the trapped-fluid region is nonlinear. For a 'linear' stratification, the circular configurations are shown to be a particular case of the family of oval modons based on a barotropic dipole and bearing a baroclinic rider, symmetric about the x-axis. These results hold also for a continuously stratified fluid ($N = const$) in the two-mode approximation.

The evolution of initially circular modons in a 'nonlinearly' (sharply) stratified two-layer fluid is generally more complicated. However, circular modons travelling relatively slowly and bearing quite strong baroclinic riders can survive for hundreds of synoptic periods while barely changing in their parameters.

In a three-layer fluid, there is a special case that can be considered without numerical simulations, but just by analogy with the two-layer dynamics. This is the case of a modon bearing a rider in the second baroclinic mode. In the absence of the first baroclinic mode, all the conclusions regarding modons in a two-layer 'linearly' stratified fluid remain valid in the three-layer model if the upper and the bottom layers are assumed to be equal in depth and twice as thin as the middle layer (the

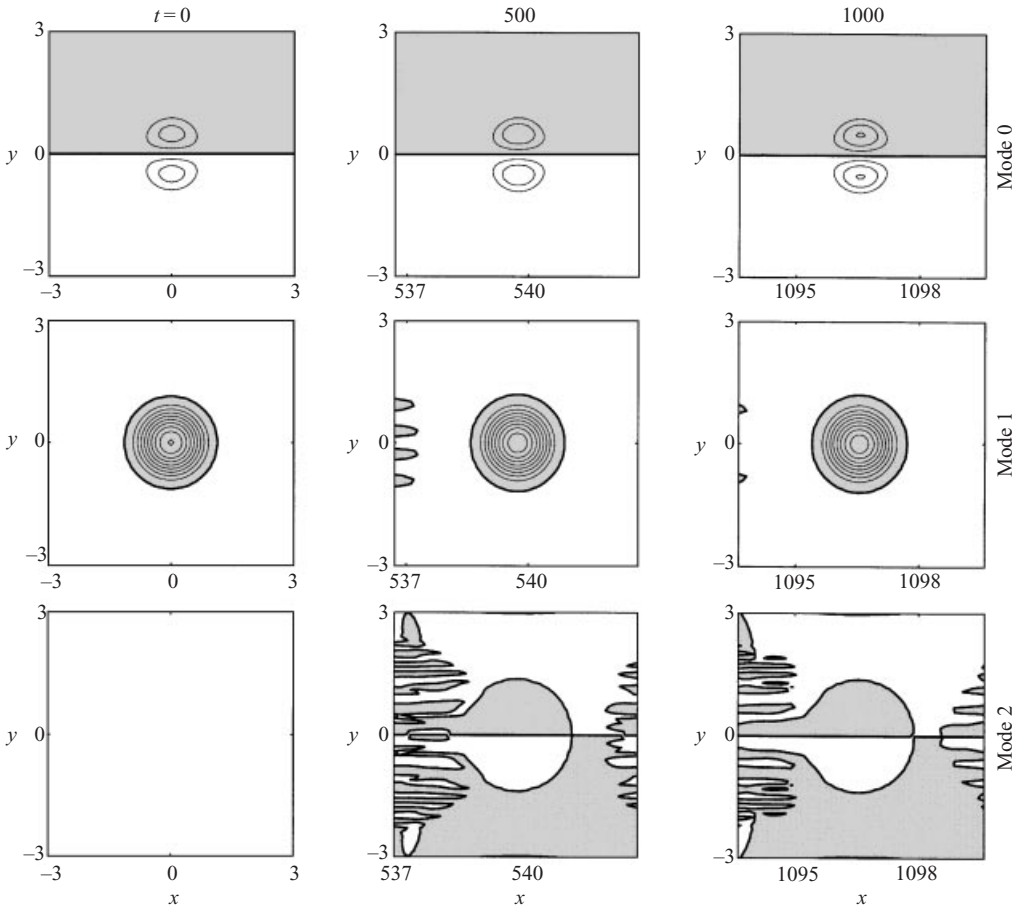

FIGURE 22. Barotropic and baroclinic PV fields at $t = 0$, 500 and 1000. The initial amplitude ratio is 3:1; other parameters as in figure 16 (designations as in figure 6).

density jumps between the layers should be equal). Accordingly, these results can be interpreted in terms of the three-mode approximations in a continuously stratified fluid. There is also an analogy between the modon dynamics in two- and three-layer sharply stratified fluids that allows us to extend the above conclusion regarding the durability of slowly translating modons to eastward-travelling quasi-monopolar intrathermocline eddies.

If the rider in a three-layer modon is coupled with the first baroclinic mode, then formally, the second baroclinic mode, antisymmetric about the x-axis, may develop. Our simulations demonstrate that, in a 'linearly' stratified three-layer fluid (i.e. when the layers are of the same depth), during the evolution of the modon, the second baroclinic mode remains negligible for a very long time (a thousand of synoptic periods at least). The circular modons bearing relatively strong riders ($A_{BC}/A_{BT} \approx 2.5$) are shown to be even more robust than those with moderate riders ($A_{BC}/A_{BT} \approx 1$). A comparison of the results obtained in the two- and three-layer models indicates that, in a continuously stratified fluid with a linear density profile, the circular dipole-plus-rider modons must be quite durable. However, to prove this statement rigorously, future numerical experiments at $n = 4, 5$, etc. are required.

While the mechanism of the first transition is clear, in principle, the processes that operate in the second transition require further explanation. Likewise, the properties of the oval modons (including their PV versus streamfunction dependence, dispersion relationships, resistance to different kinds of perturbations, etc.) require more detailed study. In this connection, the problem of constructing analytical or high-accuracy numerical stationary elliptical modon solutions is of considerable importance.

This research was supported by The Israel Science Foundation (grant 616/00). We are grateful to G. M. Reznik for stimulating discussions. We also wish to thank V. M. Kamenkovich and two other anonymous referees for helpful comments on the manuscript.

REFERENCES

Berestov, A. L. 1979 Solitary Rossby waves. *Izv. Akad. Nauk. SSSR, Atmos. Oceanic Phys.* **15**, 648–651.

Berestov, A. L. 1981 Some new solutions for the Rossby solitons. *Izv. Akad. Nauk. SSSR, Atmos. Oceanic Phys.* **17**, 82–87.

Boyd, J. P. & Ma, H. 1990 Numerical study of elliptical modons using spectral methods. *J. Fluid Mech.* **221**, 597–611.

Buchwald, V. T. 1973 Long period divergent planetary waves. *Geophys. Fluid Dyn.* **5**, 359–367.

Butchart, N., Haines, K. & Marshall, J. C. 1989 A theoretical and diagnostic study of solitary waves and atmospheric blocking. *J. Atmos. Sci.* **46**, 2063–2078.

Feliks, Y. 1990 Isolated vortex evolution in 2 and 4 mode models. *Deep-Sea Res.* **37**, 571–591.

Feliks, Y. & Ghil, M. 1993 Downwelling-front instability and eddy formation in the Eastern Mediterranean. *J. Phys. Oceanogr.* **23**, 61–78.

Feliks, Y. & Ghil, M. 1996 Mixed barotropic–baroclinic eddies growing on an eastward midlatitude jet. *Geophys. Astrophys. Fluid Dyn.* **82**, 137–171.

Feliks, Y. & Itzikowitz, S. 1987 Movement and geographical distribution of anticyclonic eddies in the Eastern Levantine Basin. *Deep-Sea Res.* **34**, 1499–1508.

Flierl, G. R., Larichev, V. D., McWilliams, J. C. & Reznik, G. M. 1980 The dynamics of baroclinic and barotropic solitary eddies. *Dyn. Atmos. Oceans* **5**, 1–41.

Flierl, G. R., Stern, M. E. & Whitehead Jr, J. A. 1983 The physical significance of modons: laboratory experiments and general integral constraints. *Dyn. Atmos. Oceans* **7**, 233–264.

van Gefen, J. H. G. M. & van Heijst, G. J. F. 1998 Viscous evolution of 2D dipolar vortices. *Fluid Dyn. Res.* **22**, 191–213.

Haines, K. & Marshall, J. C. 1987 Eddy forced coherent structures as a prototype of atmospheric blocking. *Q. J. R. Met. Soc.* **113**, 681–704.

Haupt, S. E., McWilliams, J. C. & Tribbia, J. J. 1993 Modons in shear flow. *J. Atmos. Sci.* **50**, 1181–1198.

Hecht, A., Pinardi, N. & Robinson, A. R. 1998 Currents, water masses, eddies and jets in the Mediterranean Levantine Basin. *J. Phys. Oceanogr.* **18**, 1320–1353.

Hesthaven, J. S., Lynov, J. P., Nielsen, A. H., Rassmussen, J. J., Schmidt, M. R., Shapiro, E. G. & Turitsyn, S. K. 1995 Dynamics of a nonlinear dipole vortex. *Phys. Fluids* **7**, 2220–2229.

Hesthaven, J. S., Lynov, J. P. & Nycander, J. 1993 Dynamics of nonstationary dipole vortices. *Phys. Fluids* A **5**, 622–629.

Hogg, N. G. & Stommel, H. M. 1985 The heton, an elementary interaction between discrete baroclinic geostrophic vortices, and its implications concerning eddy heat-flow. *Proc. R. Soc. Lond.* A **397**, 1–20.

Hooker, S. B., Brown, J. W., Kirwan, A. D. Jr, Lindemann, G. J. & Mied, R. P. 1995 Kinematics of a warm-core dipole ring. *J. Geophys. Res.* **100**(C12), 24 797–24 809.

Hopfinger, E. J. & van Heijst, G. J. F. 1993 Vortices in rotating fluids. *Annu. Rev. Fluid. Mech.* **25**, 241–289.

Ikeda, M. & Emery, W. J. 1984 Satellite observations and modelling of meanders in the California current system off Oregon and Nothern California. *J. Phys. Oceanogr.* **14**, 1434–1450.

Ikeda, M., Mysak, L. A. & Emery, W. J. 1984 Observation and modelling of satellite-sensed meanders and eddies off Vancouver Island. *J. Phys. Oceanogr.* **14**, 3–20.

Kamenkovich, V. M., Koshlyakov, M. N. & Monin, A. S. 1986 *Synoptic Eddies in the Ocean.* Reidel, The Netherlands, 475 pp.

Kamke, E. 1959 *Differential Gleihungen. Losungsmethoden und Losungen. I Gewohnliche Differentialgleichungen*, 6th edn. Leipzig, 546 pp.

Kizner, Z. I. 1984*a* Rossby solitons with axisymmetric baroclinic modes. *Dokl. Akad. Nauk. SSSR.* **275**, 1495–1498.

Kizner, Z. I. 1984*b* A class of exact solutions of the quasigeostrophic vorticity equation for the baroclinic ocean. In *The Thin Structure and Synoptic Variability of Seas and Oceans.* Reports of the II All-Union Symposium, part 2. Pp. 19–21, Tallin.

Kizner, Z. I. 1986*a* Strongly nonlinear solitary Rossby waves. *Oceanology* **26**, 382–388.

Kizner, Z. I. 1986*b* Intensity of synoptic eddies and the quasigeostrophic approximation. *Oceanology* **264**, 28–35.

Kizner, Z. I. 1988 On the theory of intrathermocline eddies. *Dokl. Akad. Nauk. SSSR* **300**, 453–457.

Kizner, Z. I. 1997 Solitary Rossby waves with baroclinic modes. *J. Mar. Res.* **55**, 671–685.

Kizner, Z. & Berson, D. 2000 Emergence of modons from collapsing vortex structures on the β-plane. *J. Mar. Res.* **58**, 375–403.

Larichev, V. D. 1974 On the internal boundary problem for the Rossby wave equation. *Izv. Akad. Nauk. SSSR, Atmos. Oceanic Phys.* **10**, 763–770.

Larichev, V. D. 1983*a* General features of nonlinear synoptic dynamics in the simple model of a barotropic ocean. *Oceanologia* **23**, 551–558.

Larichev, V. D. 1983*b* Qualitative analysis of nonlinear evolution of localized perturbations on a β-plane. *Oceanologia* **23**, 1303–1311.

Larichev, V. D. & Reznik, G. M. 1976*a* Two-dimensional solitary Rossby waves. *Rep. Akad. Nauk. SSSR* **231**, 1077–1080.

Larichev, V. D. & Reznik, G. M. 1976*b* Strongly nonlinear two-dimensional solitary Rossby waves. *Oceanologia* **16**, 961–967.

Larichev, V. D. & Reznik, G. M. 1982 Numerical experiments on the study of collision of two-dimensional solitary Rossby waves. *Dokl. Akad. Nauk. SSSR* **264**, 229–233.

Larichev, V. D. & Reznik, G. M. 1983 Colliding two-dimensional solitary Rossby waves. *Oceanologia* **23**, 725–734.

McWilliams, J. C., Flierl, G. R., Larichev, V. D. & Reznik, G. M. 1981 Numerical studies of barotropic modons. *Dyn. Atmos. Oceans* **5**, 219–238.

McWilliams, J. C. & Zabusky, N. J. 1982 Interactions of isolated vortices. I: Modons colliding with modons. *Geophys. Astrophys. Fluid Dyn.* **19**, 207–227.

Makino, M., Kamimura, T. & Taniuti, T. 1981 Dynamics of two-dimensional solitary vortices in a low-β-plasma with convective motion. *J. Phys. Soc. Japan* **50**, 980–989.

McWilliams, J. C. 1980 An application of equivalent modons to atmospheric blocking. *Dyn. Atmos. Oceans* **5**, 43–46.

McWilliams, J. C. & Flierl, G. R. 1979 On the evolution of isolated, nonlinear vortices. *J. Phys. Oceanogr.* **9**, 1155–1182.

Mezinger, F. & Arakawa, A. 1976 Numerical models used in atmospheric models. *GARP Publication Series* **17**, 430.

Mied, R. P. & Lindemann, G. J. 1982 The birth and evolution of eastward-propagating modons. *J. Phys. Oceanogr.* **12**, 213–230.

Morel, Y. & McWilliams, J. 1997 Evolution of isolated interior vortices in the ocean. *J. Phys. Oceanogr.* **27**, 727–748.

Nycander, J. 1992 Refutation of stability proofs for dipole vortices. *Phys. Fluids* A **4**, 467–476.

Olson, D. B. 1980 The physical oceanography of two rings observed by the cyclonic ring experiment. Part II: Dynamics. *J. Phys. Oceanogr.* **10**, 514–528.

Olson D. 1991 Rings in the ocean. *Annu. Rev. Earth Planet. Sci.* **19**, 238–311.

Pakyari, A. & Nycander, J. 1996 Steady two-layer vortices on the beta-plane. *Dyn. Atmos. Oceans* **25**, 67–86.

Reznik, G. M. 1985 An exact solution for the two-dimensional topographic solitary wave. *Dokl. Akad. Nauk. SSSR* **285**, 981–985.

Reznik, G. M., Grimshaw, R. & Sriskandarajah, K. 1997 On the evolution of two-layer localized quasigeostrophic vortices on a beta-plane. *Geophys. Astrophys. Fluid Dyn.* **86**, 1–42.

Richardson, P. L. 1983*a* Eddy kinetic energy in the North Atlantic from surface drifters. *J. Geophys. Res.* **88**, 4355–4367.

Richardson, P. L. 1983*b* Gulf-stream rings. In *Eddies in Marine Science* (ed. A. R. Robinson), pp. 19–45. Springer.

Samarsky, A. A. 1989 *Theory of Finite-Difference Schemes.* Nauka, Moscow, 616 pp.

Stern, M. E. 1975 Minimal properties of planetary eddies. *J. Mar. Res.* **33**, 1–13.

Swenson, M. 1987 Instability of equivalent-barotropic riders. *J. Phys. Oceanogr.* **17**, 492–506.

Tribbia, J. J. 1984 Modons in spherical geometry. *Geophys. Astrophys. Fluid Dyn.* **30**, 131–168.

Velasco Fuentes, O. U. & van Heijst, G. J. F. 1994 Experimental study of dipolar vortices on a topographic β-plane. *J. Fluid. Mech.* **259**, 79–106.

Velasco Fuentes, O. U. & van Heijst, G. J. F. 1995 Collision of dipolar vortices on a β-plane. *Phys. Fluids* **7**, 2735–2750.

Verkley, W. T. M. 1984 The construction of barotropic modons on a sphere. *J. Atmos. Sci.* **41**, 2492–2504.

Wirtki, K., Magaard, L. & Hager, J. 1976 Eddy energy in the oceans. *J. Phys. Oceanogr.* **12**, 746–749.